



# Connectivity as a universal predictor of tau progression in atypical Alzheimer's disease

Hannah de Bruin,<sup>1,2,3</sup> Colin Groot,<sup>1,2,4</sup> Henryk Barthel,<sup>5</sup> Gérard N. Bischof,<sup>6,7</sup> Ganna Blazhenets,<sup>8</sup> Ronald Boellaard,<sup>9,10</sup> Baayla D. C. Boon,<sup>1,11</sup> Matthias Brendel,<sup>12,13,14,15,16</sup> David M. Cash,<sup>17,18</sup> William Coath,<sup>17</sup> Gregory S. Day,<sup>11</sup> Bradford C. Dickerson,<sup>19</sup> Elena Doering,<sup>7,20</sup> Alexander Drzezga,<sup>6,7,20</sup> Christopher H. van Dyck,<sup>21,22</sup> Thilo van Eimeren,<sup>7,23</sup> Wiesje M. van der Flier,<sup>1,2</sup> Carolyn A. Fredericks,<sup>24,25</sup> Tim D. Fryer,<sup>26,27</sup> Elsmarieke van de Giessen,<sup>9,10</sup> Brian A. Gordon,<sup>28,29</sup> Jonathan Graff-Radford,<sup>30</sup> Lea T. Grinberg,<sup>8,31</sup> Oskar Hansson,<sup>4</sup> Diana A. Hobbs,<sup>28,29</sup> Merle C. Hoenig,<sup>6,7</sup> Günter Höglinger,<sup>13,14,32</sup> David J. Irwin,<sup>33,34</sup> P. Simon Jones,<sup>26</sup> Keith A. Josephs,<sup>30</sup> Yuta Katsumi,<sup>19</sup> Renaud La Joie,<sup>8</sup> Edward B. Lee,<sup>35,36,37</sup> Johannes Levin,<sup>13,14,32</sup> Maura Malpetti,<sup>26,38</sup> Scott M. McGinnis,<sup>19</sup> Adam P. Mecca,<sup>21,22</sup> Rosaleena Mohanty,<sup>39</sup> Ilya M. Nasrallah,<sup>40</sup> John T. O'Brien,<sup>41</sup> Ryan S. O'Dell,<sup>21,22</sup> Carla Palleis,<sup>32</sup> Robert Perneczky,<sup>42</sup> Jeffrey S. Phillips,<sup>33,34</sup> Deepti Putcha,<sup>19</sup> Gil D. Rabinovici,<sup>8,43</sup> Nesrine Rahmouni,<sup>44</sup> Pedro Rosa-Neto,<sup>44</sup> James B. Rowe,<sup>26,45</sup> Michael Rullmann,<sup>5</sup> Osama Sabri,<sup>5</sup> Dorothee Saur,<sup>46</sup> Andreas Schildan,<sup>5</sup> Jonathan M. Schott,<sup>17</sup> Matthias L. Schroeter,<sup>47,48</sup> William W. Seeley,<sup>8,31</sup> Stijn Servaes,<sup>44</sup> Irene Sintini,<sup>49</sup> Ruben Smith,<sup>4,50</sup> Salvatore Spina,<sup>8</sup> Jenna Stevenson,<sup>44</sup> Erik Stomrud,<sup>4,50</sup> Olof Strandberg,<sup>4</sup> Joseph Theriault,<sup>44</sup> Pontus Tideman,<sup>4,50</sup> Alexandra Touroutoglou,<sup>19</sup> Anne E. Trainer,<sup>51</sup> Denise Visser,<sup>2,9,10</sup> Fattin Wekselman,<sup>8,31</sup> Philip S. J. Weston,<sup>17,18</sup> Jennifer L. Whitwell,<sup>49</sup> David A. Wolk,<sup>33,35,52</sup> Keir Yong,<sup>17</sup> Yolande A. L. Pijnenburg,<sup>1,2</sup> Nicolai Franzmeier,<sup>3,13,53,†</sup> and Rik Ossenkoppele<sup>1,2,4,†</sup> for the Alzheimer's Disease Neuroimaging Initiative (ADNI)

<sup>†</sup>These authors contributed equally to this work.

See Malotiaux et al. (<https://doi.org/10.1093/brain/awaf350>) for a scientific commentary on this article.

The link between regional tau load and clinical manifestation of Alzheimer's disease (AD) highlights the importance of characterizing spatial tau distribution across disease variants. In typical (memory-predominant) AD, the spatial progression of tau pathology mirrors the functional connections from temporal lobe epicentres. However, given the limited spatial heterogeneity of tau in typical AD, atypical (non-amnesic-predominant) AD variants with distinct tau patterns provide a key opportunity to investigate the universality of connectivity as a scaffold for tau progression. In this large-scale, multicentre study across 14 international sites, we included cross-sectional tau-PET data from 320 individuals with atypical AD ( $n = 139$  posterior cortical atrophy/PCA-AD;  $n = 103$  logopenic variant primary progressive aphasia/lvPPA-AD;  $n = 35$  behavioural variant AD/bvAD;  $n = 43$  corticobasal syndrome/CBS-AD), with a subset of individuals ( $n = 78$ ) having longitudinal tau-PET data. Additionally, as an independent sample, we included regional post-mortem tau stainings from 93 atypical AD patients from two sites ( $n = 19$  PCA-AD,  $n = 32$  lvPPA-AD,  $n = 23$

Received March 05, 2025. Revised May 30, 2025. Accepted July 13, 2025. Advance access publication August 14, 2025

© The Author(s) 2025. Published by Oxford University Press on behalf of the Guarantors of Brain.

This is an Open Access article distributed under the terms of the Creative Commons Attribution License (<https://creativecommons.org/licenses/by/4.0/>), which permits unrestricted reuse, distribution, and reproduction in any medium, provided the original work is properly cited.

bvAD,  $n = 19$  CBS-AD). Gaussian mixture modelling was used to harmonize different tau-PET tracers by transforming tau-PET standardized uptake value ratios to tau positivity probabilities (a uniform scale ranging from 0% to 100%). Using linear regression, we assessed whether brain regions with stronger resting-state functional MRI-based functional connectivity, derived from healthy elderly controls in the Alzheimer's Disease Neuroimaging Initiative (ADNI), showed greater covariance in cross-sectional and longitudinal tau-PET and post-mortem tau pathology. Furthermore, we examined whether functional connectivity of tau-PET epicentres (i.e. the top 5% of regions with the highest baseline tau load) and tau-PET accumulation epicentres (i.e. the top 5% of regions with the highest tau accumulation rates) was associated with cross-sectional and longitudinal tau patterns.

Our findings show that tau-PET epicentres aligned with clinical variants, e.g. a visual network predominant pattern in PCA-AD ('visual AD') and left-hemispheric temporal predominance, particularly within the language network, in lvPPA-AD ('language AD'). Moreover, more strongly functionally connected regions showed correlated concurrent tau-PET levels (confirmed with post-mortem data) and tau-PET accumulation rates. The functional connectivity profile of tau-PET epicentres and accumulation epicentres corresponded to tau-PET progression patterns, with higher tau-PET levels and accumulation rates in functionally close regions, and lower tau-PET levels and accumulation rates in functionally distant regions.

Our data are consistent with the hypothesis that tau propagation occurs along functional connections originating from local epicentres, across all AD clinical variants. Since tau proteinopathy is a major driver of neurodegeneration and cognitive decline, this finding may advance personalized medicine and participant-specific end points in clinical trials.

- 1 Alzheimer Center Amsterdam, Neurology, Vrije Universiteit Amsterdam, Amsterdam UMC Location VUmc, Amsterdam 1081 HV, The Netherlands
- 2 Amsterdam Neuroscience, Neurodegeneration, Amsterdam 1081 HV, The Netherlands
- 3 Institute for Stroke and Dementia Research (ISD), University Hospital, Ludwig Maximilian University of Munich, Munich 81377, Germany
- 4 Clinical Memory Research Unit, Department of Clinical Sciences Malmö, Faculty of Medicine, Lund University, Lund 221 00, Sweden
- 5 Department of Nuclear Medicine, University of Leipzig, Leipzig 04109, Germany
- 6 Research Center Jülich, Institute for Neuroscience and Medicine II, Molecular Organization of the Brain, Jülich 52428, Germany
- 7 Faculty of Medicine and University Hospital Cologne, Department of Nuclear Medicine, University of Cologne, Cologne 50923, Germany
- 8 Department of Neurology, Memory and Aging Center, Weill Institute for Neurosciences, University of California, San Francisco, San Francisco, CA 94158, USA
- 9 Radiology & Nuclear Medicine, Vrije Universiteit Amsterdam, Amsterdam UMC Location VUmc, Amsterdam 1081 HV, The Netherlands
- 10 Amsterdam Neuroscience, Brain Imaging, Amsterdam 1081 HV, The Netherlands
- 11 Neurology/neuropathology, Mayo Clinic, Jacksonville, FL 32224, USA
- 12 Department of Nuclear Medicine, LMU University Hospital, Munich 81377, Germany
- 13 Munich Cluster for Systems Neurology (SyNergy), Munich 81377, Germany
- 14 German Center for Neurodegenerative Diseases (DZNE), Munich 81377, Germany
- 15 German Cancer Consortium (DKTK), Partner Site Munich, a Partnership Between German Cancer Research Center (DKFZ) and LMU Munich, Munich 81377, Germany
- 16 Bavarian Cancer Research Center (BZKF), Partner Site Munich, Munich 81377, Germany
- 17 Dementia Research Centre, UCL Queen Square Institute of Neurology, London WC1N 3BG, UK
- 18 UK Dementia Research Institute, UCL, London NW1 3BT, UK
- 19 Frontotemporal Disorders Unit, Department of Neurology, Massachusetts General Hospital and Harvard Medical School, Boston, MA 02114, USA
- 20 German Center for Neurodegenerative Diseases (DZNE), Bonn/Cologne 53127, Germany
- 21 Alzheimer's Disease Research Unit, Yale University School of Medicine, New Haven, CT 06510, USA
- 22 Department of Psychiatry, Yale University School of Medicine, New Haven, CT 06510, USA
- 23 Department of Neurology, Faculty of Medicine and University Hospital Cologne, University of Cologne, Cologne 50937, Germany
- 24 Department of Neurology, Yale University School of Medicine, New Haven, CT 06510, USA
- 25 Department of Neurology, Yale New Haven Hospital, New Haven, CT 06510, USA
- 26 Department of Clinical Neurosciences and Cambridge University Hospitals NHS Trust, University of Cambridge, Cambridge CB2 0QQ, UK
- 27 Wolfson Brain Imaging Centre, University of Cambridge, Cambridge CB2 0QQ, UK

- 28 Department of Radiology, Washington University in St Louis, St Louis, MO 63130, USA  
29 Knight Alzheimer's Disease Research Center, Washington University in St Louis, St Louis, MO 63130, USA  
30 Department of Neurology, Mayo Clinic, Rochester, MN 55905, USA  
31 Department of Pathology, University of California, San Francisco, San Francisco, CA 94143, USA  
32 Department of Neurology, LMU University Hospital, LMU Munich, Munich 81377, Germany  
33 Department of Neurology, University of Pennsylvania, Philadelphia, PA 19104, USA  
34 Penn Frontotemporal Degeneration Center, University of Pennsylvania, Philadelphia, PA 19104, USA  
35 Institute on Aging, University of Pennsylvania, Philadelphia, PA 19104, USA  
36 Department of Pathology & Laboratory Medicine, University of Pennsylvania, Philadelphia, PA 19104, USA  
37 Center for Neurodegenerative Disease Research, Perelman School of Medicine, University of Pennsylvania, Philadelphia, PA 19104, USA  
38 Department of Clinical Neurosciences, UK Dementia Research Institute at the University of Cambridge, Cambridge CB2 0AH, UK  
39 Division of Clinical Geriatrics, Center for Alzheimer Research, Department of Neurobiology, Karolinska Institutet, Huddinge 141 83, Sweden  
40 Department of Radiology, University of Pennsylvania, Philadelphia, PA 19104, USA  
41 Department of Psychiatry, University of Cambridge, Cambridge CB2 0SZ, UK  
42 Department of Psychiatry and Psychotherapy, LMU University Hospital, Munich 80336, Germany  
43 Department of Radiology and Biomedical Imaging, University of California, San Francisco, San Francisco, CA 94143, USA  
44 McGill Centre for Studies in Aging, Department of Neurology and Neurosurgery, McGill University, Montreal, QC H3A 2B4, Canada  
45 Medical Research Council Cognition and Brain Sciences Unit, Cambridge CB2 7EF, UK  
46 Department of Neurology, University of Leipzig, Leipzig 04103, Germany  
47 Clinic for Cognitive Neurology, University of Leipzig, Leipzig 04103, Germany  
48 Department of Neurology, Max Planck Institute for Human Cognitive and Brain Sciences, Leipzig 04103, Germany  
49 Department of Radiology, Mayo Clinic, Rochester, MN 55905, USA  
50 Memory Clinic, Skåne University Hospital, Malmö 205 02, Sweden  
51 Clinical Neurosciences Imaging Center, Yale University School of Medicine, New Haven, CT 06510, USA  
52 Penn Memory Center, University of Pennsylvania, Philadelphia, PA 19104, USA  
53 The Sahlgrenska Academy, Institute of Neuroscience and Physiology, Psychiatry and Neurochemistry, University of Gothenburg, Gothenburg 413 90, Sweden

Correspondence to: Hannah de Bruin

Alzheimer Center Amsterdam, Neurology, Vrije Universiteit Amsterdam, Amsterdam UMC Location VUmc, De Boelelaan 1118, Amsterdam 1081 HV, Noord-Holland, The Netherlands

E-mail: h.debruin1@amsterdamumc.nl

Correspondence may also be addressed to: Rik Ossenkoppele

De Boelelaan 1118, 1081 HV Amsterdam, The Netherlands

E-mail: r.ossenkoppele@amsterdamumc.nl

**Keywords:** atypical Alzheimer's disease; heterogeneity; tau; connectivity; PET; fMRI

## Introduction

The main pathological hallmarks of Alzheimer's disease (AD) are extracellular amyloid- $\beta$  (A $\beta$ ) plaques and intracellular tau neurofibrillary tangles (NFTs).<sup>1</sup> Previous studies have consistently shown that compared with A $\beta$  proteinopathy, tau proteinopathy is both spatially and temporally more strongly associated with neurodegeneration and cognitive impairment.<sup>2–4</sup> This highlights the critical role of tau pathology in AD progression and the importance of better understanding how tau spreads throughout the brain.

Preclinical and human neuroimaging studies have indicated that the brain's connectome acts as a scaffold for the progression of tau across the brain.<sup>4–26</sup> Specifically, tau may originate in specific local epicentres (i.e. the regions with the earliest and greatest tau burden), from where it spreads along the connections of these epicentres.<sup>5,7,13,16–21,27</sup> On the other hand, functionally connected regions may also share vulnerability through commonalities in

metabolic- and activity-dependent stresses, gene expression and proteostasis.<sup>28</sup> These studies collectively provide robust evidence that connectivity plays a crucial role in the progression of tau pathology throughout the brain. However, previous clinical studies have primarily focused on individuals with typical AD, who present with an amnesic-predominant clinical syndrome. Although there are inter-individual differences in typical AD, the spatial heterogeneity of tau is generally limited,<sup>7,8,19,29</sup> and largely adheres to the Braak staging scheme of tau pathology with a strong emphasis on medial and lateral aspects of the temporal lobe.<sup>1,30–34</sup> Therefore, a crucial test of the connectivity-progression hypothesis is to determine whether connectivity-based tau progression models can be generalized to clinical phenotypes with other tau deposition patterns extending beyond the temporal lobe. Notable phenotypes of interest for this purpose are so-called atypical variants of AD, including posterior cortical atrophy (PCA: the 'visual variant of AD'),<sup>35</sup> logopenic variant primary progressive aphasia (lvPPA: the 'language variant



of AD'),<sup>36</sup> behavioural variant AD (bvAD)<sup>37</sup> and corticobasal syndrome (CBS: the 'motor variant of AD').<sup>38</sup> Each of these variants shows distinct spatial tau patterns that largely correspond to the regions governing the cognitive functions that define each variant. In particular, the primary visual cortex and visual association areas show prominent tau burden in PCA; the left superior temporal gyrus in lvPPA; temporoparietal and to a lesser extent frontal regions in bvAD; and predominantly the hemisphere contralateral to the clinically affected body side, including the sensorimotor cortex, in CBS.<sup>5,16,20,39–44</sup> It is, therefore, of both scientific and clinical interest to better understand the mechanisms that drive heterogeneous tau progression patterns and subsequent clinical variability in AD.

To test whether functional connectivity is a universal predictor of tau progression, independent of clinical phenotype, we aimed to assess tau-PET progression patterns as well as post-mortem tau distributions in Aβ-positive individuals with PCA, lvPPA, bvAD, CBS and typical AD. Because atypical AD variants are relatively rare,<sup>45,46</sup> we conducted a large-scale multicentre study on atypical AD, using patient-specific tau-PET across 14 sites worldwide ( $n = 320$ , with  $n = 68$  typical AD cases serving as the benchmark group) and resting-state functional MRI (fMRI) data from healthy elderly controls in the Alzheimer's Disease Neuroimaging Initiative [ADNI,  $n = 42$  cognitively normal (CN) Aβ-negative individuals], as well as post-mortem datasets from two sites [University of Pennsylvania (UPENN)  $n = 63$ , University of California, San Francisco (UCSF)  $n = 30$ ]. Our objectives were to: (i) assess the spatial heterogeneity of tau-PET distribution and identify subject-level tau-PET epicentres across AD variants; (ii) test whether brain regions with stronger functional connectivity to each other show greater covariance in cross-sectional tau-PET and gold standard post-mortem tau pathology; (iii) assess whether functional connectivity of subject-level tau-PET epicentres (i.e. regions with the highest tau at baseline) predicts cross-sectional tau patterns; (iv) test whether brain regions with stronger functional connectivity to each other show greater covariance in tau-PET accumulation rates; and (v) establish whether functional connectivity of subject-level tau-PET accumulation epicentres (i.e. regions with the highest accumulation of tau over time) predicts longitudinal tau progression sequences. We hypothesize that, in all clinical variants of AD, tau propagates along functional connections of the subject-level tau-PET epicentre (i.e. the regions with the highest tau-PET level or fastest tau-PET accumulation), indicating a universal scaffold for the progression of tau pathology. In addition, we hypothesize that brain regions with stronger functional connectivity to each other show stronger covariance in tau pathology on post-mortem examination. By investigating the association between tau and functional connectivity this study aims to deepen the understanding of mechanisms of tau progression and AD heterogeneity, potentially informing more targeted therapeutic strategies and tailored clinical trial end points.

## Materials and methods

### Tau-PET sample

We included individuals with AD recruited at 14 international sites [Amsterdam, Cambridge, Cologne, Leipzig, Lund, Mayo, Massachusetts General Hospital (MGH), McGill, Munich, University College London (UCL), UCSF, UPENN, Washington and Yale]. Inclusion criteria were a clinical diagnosis of atypical AD according to the contemporaneously available criteria,<sup>35–38</sup> confirmed positive Aβ status (either via PET or CSF), and the availability of at least one

tau-PET scan and basic demographic and clinical information. We also received data from several sites on individuals with typical AD, whom we decided to include as a reference group. Longitudinal tau-PET data was available for a subset of individuals within each AD variant. However, due to the relatively small sample sizes in the other variants, we only included this data for PCA-AD and lvPPA-AD. In addition to data from AD patients, we also obtained data from control subjects (primarily consisting of CN Aβ-negative individuals) scanned using the same tau-PET tracers. This ensured the inclusion of varying tau-PET levels at both the lower and higher ends of the spectrum, enabling Gaussian mixture modelling-based transformation of tau-PET standardized uptake value ratio (SUVR) values to tau positivity probabilities<sup>7</sup> (see [Supplementary material](#), 'Methods' section). Besides control data from the aforementioned 14 cohorts, we also included control data from ADNI for this. All study procedures were conducted in accordance with the Declaration of Helsinki, ethical approval was obtained by investigators at each site. All study participants provided written informed consent.

### Neuroimaging data collection

Every individual underwent at least one tau-PET scan following site-specific acquisition protocols.<sup>4,14,16,47–57</sup> Both scanning protocols and specific tracers varied by site, with tracers including <sup>18</sup>F-flortaucipir, <sup>18</sup>F-MK6240, <sup>18</sup>F-PI2620 and <sup>18</sup>F-RO948. Before data pre-processing, all imaging data were reviewed for artefacts and image quality.

Preprocessing steps and region-of-interest (ROI) extraction were performed either centrally (in Amsterdam/Munich) or locally. Collaborators from Cambridge, Cologne, Lund, Mayo, MGH, McGill, UCL, UCSF, UPENN, and Washington conducted both pre-processing and ROI extraction at their respective sites.<sup>4,14,16,48,50–52,54–56</sup> PET scans from Leipzig, Yale, Amsterdam and Munich were centrally analysed.<sup>47,49</sup> To ensure consistency across all sites, ROI extraction followed a standardized protocol: each site was provided with an R script, the Schaefer parcellation and a grey matter mask, which were used to generate the Schaefer 200 values: [https://github.com/OssenKoppeLab/HdeBruin\\_Atypical\\_AD](https://github.com/OssenKoppeLab/HdeBruin_Atypical_AD).

For preprocessing, individual PET scan frames were realigned and averaged to create average images, which were subsequently co-registered to the corresponding T1-weighted MRI. For ROI extraction, the cortical Schaefer atlas<sup>58</sup> with 200 ROIs applied to the structural MRI image was used to extract regional tau-PET SUVR data, which was adjusted to an inferior cerebellar grey reference region.

### Assessment of tau-PET change

We assessed tau-PET change over time by computing the annual SUVR change for every individual across 200 ROIs. For each individual and each ROI, we fitted a separate linear model defined as:  $\text{tau-PET SUVR} = \beta_0 + \beta_1 \times \text{time} + \epsilon$ , where tau-PET SUVR reflects the tau load at a given time point,  $\beta_0$  is the intercept,  $\beta_1$  is the slope, time is the follow-up time in years and  $\epsilon$  is the residual error term. To express the change as a relative percentage, we normalized each ROI's slope ( $\beta_1$ ) by the individual's baseline SUVR for that ROI (i.e. at follow-up time = 0):  $\text{relative tau-PET change (\% per year)} = (\beta_1 / \text{tau-PET SUVR}_0) \times 100$ . This yielded the annual percentage change in tau-PET signal per ROI.

### Identification of tau-PET epicentres

To determine the tau-PET epicentre for each individual, we employed a previously established method<sup>7,19,59</sup> that is based on the

premise that brain regions showing early abnormal tau deposition would display higher tau levels than regions with later abnormal tau deposition. At the subject level, we arranged all Schaefer ROIs according to their tau-PET SUVR values at baseline, thereby delineating the estimated cross-sectional sequence of tau propagation. Subject-specific tau epicentres were then defined as the top 5% of ROIs (i.e. 10 ROIs in total) with the highest tau-PET SUVR values. We determined tau-PET accumulation epicentres in a similar way, see [Supplementary material](#), 'Methods' section.

### Post-mortem sample

As an independent sample (i.e. not the same individuals as in the tau-PET sample), we recruited data from AD cases who had undergone post-mortem examination at two sites (UPENN and UCSF).<sup>60,61</sup> Inclusion criteria were an ante-mortem clinical diagnosis of atypical AD, AD being the primary neuropathological diagnosis, the availability of post-mortem ordinal or quantitative tau assessments in preferably ~10 probe extraction sites per individual including their anatomical labelling, and the presence of basic demographic and ante-mortem clinical information.

### Post-mortem assessment

Post-mortem data collection and preparation followed standard pre-established procedures.<sup>60,61</sup> All assessments were unilateral (see [Supplementary methods](#)). UPENN tau assessments included ordinal ratings (0 = none, 1 = mild, 2 = moderate, 3 = severe) of paired helical filament-1 (PHF-1) staining<sup>62</sup> across 19 ROIs (i.e. the amygdala, dentate gyrus, CA1/subiculum, entorhinal cortex, middle frontal cortex, angular gyrus, superior/middle temporal cortex, anterior cingulate, occipital cortex, caudate/putamen, globus pallidus, thalamus/subthalamic nucleus, midbrain, substantia nigra, pons, locus coeruleus, medulla, cerebellum and sensory cortex). From these ROIs, we selected those with sufficient data and relevance for assessing functional connectivity for our fMRI-based analyses. Additionally, due to the small size of individual hippocampal regions, we combined these into a single hippocampal ROI. This selection narrowed the 19 ROIs down to 9: the amygdala, hippocampus, entorhinal cortex, middle frontal cortex, angular gyrus, superior/middle temporal cortex, anterior cingulate, occipital cortex, thalamus/subthalamic nucleus. UCSF tau assessments consisted of quantitative thioflavin-S fluorescent microscopy staining<sup>61</sup> across six ROIs (i.e. the CA1, subiculum, middle frontal gyrus, angular gyrus, superior temporal gyrus and primary motor cortex), resulting in a density score (i.e. the number of NFTs per mm<sup>2</sup>) per ROI. All six ROIs had sufficient data and were fMRI compatible. We again combined the individual hippocampal regions into a single hippocampal ROI, resulting in five total ROIs. For both samples, we used known cortical and subcortical brain atlases [i.e. the automated anatomical labelling (AAL) atlas, computational brain anatomy laboratory (CoBrA) atlas, Julich atlas and Neuromorphometrics atlas]<sup>63–66</sup> to create an MRI brain atlas based on the selected ROIs.<sup>67</sup> Although pathology assessments were unilateral, ROIs were mapped bilaterally in the atlas to align with the functional connectivity analyses.

### Assessment of covariance in tau-PET and covariance in post-mortem tau

Cross-sectional and longitudinal tau-PET covariance were defined as AD variant-average Fisher z-transformed partial Pearson

correlations between, respectively, tau positivity probabilities or tau-PET SUVR percentage change rates of all 200 Schaefer ROI pairs, while adjusting for age, sex, site (and Euclidean distance). We assessed tau-PET covariance both across the whole brain and in seven individual canonical resting-state fMRI networks.<sup>68</sup> Post-mortem tau covariance was determined by calculating Fisher z-transformed partial Spearman (UPENN) and Pearson (UCSF) correlations between post-mortem tau semi-quantitative and quantitative ratings of all ROI pairs (based on the created bilateral MRI brain atlas), respectively, while adjusting for age and sex.

### Functional connectivity assessment

We utilized resting-state fMRI data from an independent sample of 42 CN Aβ-negative individuals from ADNI to construct the connectome template, along which tau progression was modelled. Pre-processing of the fMRI data involved several steps, starting with slice-timing correction and motion correction, with all volumes realigned to the first volume. Echo planar imaging (EPI) images were subsequently co-registered to their respective T1-weighted structural scans. Grey matter, eroded white matter and eroded CSF segments derived from the T1 images were transformed into EPI space based on rigid transformation parameters.

To denoise the fMRI data, we regressed out nuisance signals, including time series from eroded white matter and CSF, as well as six motion parameters. Additional steps included detrending and band-pass filtering within the 0.01–0.08 Hz frequency range, with all processing conducted in native EPI space. To minimize the impact of motion artefacts on connectivity estimates, motion scrubbing was performed. Volumes with frame-wise displacement above 0.5 mm, along with one preceding and two following volumes, were excluded. Each participant retained at least 5 min of usable resting-state fMRI data after scrubbing. Spatial smoothing was avoided to prevent artificial enhancement of connectivity signals due to spatial overlap (and thus, spilling) between neighbouring brain regions. Finally, the pre-processed resting-state fMRI data were warped to Montreal Neurological Institute (MNI) space using spatial normalization parameters from CAT12.

Subsequently, for the tau-PET part of this study, we applied the 200 ROI Schaefer atlas to the fMRI data to generate a functional connectivity matrix representing Fisher z-transformed Pearson correlations between fMRI time series [i.e. fluctuations in the blood oxygen level-dependent (BOLD) signal] of all possible ROI pairs. Based on a previously established method, this matrix was density thresholded at 30% (i.e. 30% of the strongest positive connections were retained) and transformed to functional connectivity-based distance.<sup>7</sup> The distance metric reflects the shortest functional path length between each ROI pair, where regions with stronger direct or indirect connections are considered closer together, and regions with weaker or no connections are considered more distant. Besides assessing functional connectivity across the whole brain, we also determined functional connectivity in the same seven canonical resting-state fMRI networks (i.e. the default mode network, dorsal and ventral attention network, frontoparietal control network, limbic network, motor network and visual network) that were used for assessing tau-PET covariance.<sup>68</sup> For the post-mortem part of this study, we applied our MRI brain atlas to the fMRI data to generate a functional connectivity matrix representing Fisher z-transformed Pearson correlations between the fMRI time series of all possible ROI pairs. We did not transform functional connectivity to functional connectivity-based distance for our post-mortem analyses due to sparsity and limited adjacency of regions.

## Statistical analyses

Group differences in baseline demographics were assessed using ANOVA or Kruskal–Wallis tests for continuous variables and chi-squared tests of independence for categorical variables. In the case of cell counts <5, Monte Carlo simulations with 20 000 replications ( $B = 20\,000$ ) were employed to estimate the  $P$ -values for the chi-squared tests. If a statistically significant main effect was observed, Tukey's Honestly Significant Difference (HSD) test was used as a post hoc test following ANOVA, Dunn's test following the Kruskal–Wallis test, and Fisher's exact tests following chi-square tests. Dunn's test and Fisher's exact tests were adjusted for multiple comparisons using the Bonferroni correction. When data was missing for a category [education  $n = 89$ , Apolipoprotein E (APOE $\epsilon$ 4) status  $n = 150$ , Mini-Mental State Examination (MMSE)  $n = 79$ ], individuals were excluded from that specific analysis. For our cross-sectional *in vivo* covariance analyses, the association between inter-regional functional connectivity-based distance and age-, sex- and site-adjusted inter-regional tau-PET covariance was assessed using linear regression for each AD variant, both in the whole brain and in the seven individual resting-state fMRI networks. As a sensitivity analysis, we repeated these analyses with additional adjustment of tau-PET covariance for inter-regional Euclidean distance (i.e. the geometric distance between the centre of mass of each ROI). Furthermore, to test the robustness of our findings, we performed a previously described bootstrapping procedure.<sup>8</sup> In this procedure, 1000 different connectivity null models were generated by shuffling the  $200 \times 200$  connectivity matrix while preserving the weight and degree distribution. Subsequently, we re-ran the whole-brain linear model 1000 times, each time using a different connectivity matrix from the set of 1000 null models. This procedure resulted in a distribution of 1000  $\beta$ -values based on the null models, which were compared against the actual  $\beta$ -value using exact tests. For our post-mortem covariance analyses, the association between inter-regional functional connectivity and age- and sex-adjusted inter-regional tau pathology covariance was also assessed using linear regression. Here, we pooled the data from all atypical AD variants to increase statistical power. To study cross-sectional *in vivo* tau progression, at the subject level, linear regression was used to assess the association between functional connectivity-based distance to the tau epicentre and tau-PET SUVR, after which  $\beta$ -values were visualized per AD variant. Additionally, we grouped all non-epicentre regions into quartiles based on their functional proximity to the epicentre (quartile 1 = close, quartile 4 = distant) and compared tau positivity probabilities across quartiles using paired Wilcoxon signed-rank tests. For our longitudinal *in vivo* covariance analyses, we assessed the association between inter-regional functional connectivity-based distance and inter-regional tau-PET annual percentage change covariance through linear regression for each AD variant, both across the whole brain and in the seven individual resting-state fMRI networks. We applied the same bootstrapping procedure used in our cross-sectional covariance analyses to evaluate the robustness of our findings. To study longitudinal *in vivo* tau progression, at the subject level, linear regression was utilized to assess the association between functional connectivity-based distance to the tau accumulation epicentre and tau-PET annual percentage change, after which  $\beta$ -values were visualized per AD variant. Moreover, we grouped all non-accumulation-epicentre regions into quartiles based on their functional proximity to the accumulation epicentre (quartile 1 = close, quartile 4 = distant) and compared tau-PET percentage change rates across quartiles using paired Wilcoxon signed-rank tests. Significance for all effects was

determined at a two-tailed  $\alpha = 0.05$ . All statistical analyses were performed using R statistical software (R Foundation for Statistical Computing, Vienna, Austria). Brain surface renderings were generated using the Connectome Workbench.

## Results

### Sample characteristics

For the tau-PET section of this study, we included 388 A $\beta$ -positive (either on PET or CSF) individuals with a clinical diagnosis of AD. For two individuals, A $\beta$  status was not known, but they were included based on a positive tau-PET scan. In total, 139 individuals were classified as PCA-AD, 103 as lvPPA-AD, 35 as bvAD, 43 as CBS-AD and 68 as typical (or amnesic) AD. Baseline tau-PET data was available for all 388 individuals. Longitudinal tau-PET data was available for 78 individuals with PCA-AD or lvPPA-AD (PCA-AD  $n = 45$ , mean follow-up time:  $1.40 \pm 0.63$  years, range: 0.77–3.16 years; lvPPA-AD  $n = 33$ , mean follow-up time:  $1.41 \pm 0.78$  years, range: 0.79–4.07 years). For the post-mortem section of this study, we included 93 individuals with an ante-mortem clinical diagnosis of atypical AD as well as post-mortem neuropathologically confirmed AD from two sites. One of these sites (UPENN) provided a larger semi-quantitative dataset ( $n = 63$ ; 12 PCA-AD, 23 lvPPA-AD, 13 bvAD and 15 CBS-AD), while the other site (UCSF) contributed a smaller quantitative dataset ( $n = 30$ ; 7 PCA-AD, 9 lvPPA-AD, 10 bvAD and 4 CBS-AD), which was used as a replication sample. Baseline demographic, clinical and imaging/neuropathological information across AD variants is presented in [Table 1](#) (tau-PET cohort) and [Table 2](#) (post-mortem cohort), while baseline demographic and clinical information across all sites can be found in [Supplementary Table 1](#).

### Tau-PET spatial distribution and epicentres align with clinical phenotypes

Our first objective was to assess the heterogeneity of tau-PET distribution and identify tau-PET epicentres across AD variants. Accordingly, similar to previous approaches,<sup>7,19</sup> and pending the development of widely accepted tau-PET harmonization methods,<sup>69</sup> we harmonized the different tau-PET tracers from the different sites by transforming tau-PET SUVRs to tau positivity probabilities (0% to 100%) using Gaussian mixture modelling. For each AD variant, we computed tau-PET positivity probabilities in 200 Schaefer atlas<sup>58</sup> ROIs ([Fig. 1B](#)). The tau positivity probability maps generally resembled the previously described topography of each clinical variant, including a posterior pattern in PCA-AD,<sup>16,35,40,70,71</sup> pronounced left-hemispheric temporal involvement in lvPPA-AD,<sup>16,36,40,72,73</sup> a diffuse pattern primarily involving the temporoparietal regions, with additional frontal involvement, in bvAD,<sup>16,37,47</sup> and bilateral temporoparietal predominance in typical AD.<sup>1,16,40</sup> The exception was the CBS-AD group, which showed a prominent posterior pattern ([Supplementary Fig. 1B](#) shows the tau positivity probabilities for individuals with CBS-AD grouped by the predominant clinically affected side). Although there was some unique involvement of the sensorimotor cortex (that was not observed in any of the other variants), this was less pronounced than in several previous studies.<sup>40,42,74,75</sup> Regional tau-PET positivity probabilities were generally lower in CBS-AD and typical AD compared with the other variants. Furthermore, in line with the spatial distribution of tau positivity probabilities, tau epicentres (i.e. the top 5% of regions exhibiting the highest baseline tau-PET SUVR, determined at the subject level) were highly heterogeneous across variants ([Fig. 1A](#) and [Supplementary Fig. 1A](#)). Correlations between the entire multisite



**Table 1 Tau-PET cohort: demographic, clinical and imaging information across atypical AD variants**

|                                | PCA-AD                        | lvPPA-AD                    | bvAD                        | CBS-AD                      | Typical AD                    | Total        | P                   |
|--------------------------------|-------------------------------|-----------------------------|-----------------------------|-----------------------------|-------------------------------|--------------|---------------------|
| N                              | 139                           | 103                         | 35                          | 43                          | 68                            | 388          |                     |
| Age (years) <sup>a</sup>       | 64.05 ± 7.66 <sup>b,c,d</sup> | 67.75 ± 8.31 <sup>d,e</sup> | 65.95 ± 8.05 <sup>c,d</sup> | 71.76 ± 8.56 <sup>e,f</sup> | 71.77 ± 9.25 <sup>b,e,f</sup> | 67.41 ± 8.79 | <0.001              |
| Female <sup>g</sup>            | 85 (61.2)                     | 52 (50.5)                   | 18 (51.4)                   | 23 (53.5)                   | 32 (47.1)                     | 210 (54.1)   | 0.310               |
| Education (years) <sup>a</sup> | 15.43 ± 2.99                  | 15.58 ± 3.38 <sup>d</sup>   | 14.68 ± 3.76                | 14.58 ± 3.49                | 13.91 ± 3.58 <sup>b</sup>     | 15.10 ± 3.36 | 0.045               |
| APOEε4 carrier <sup>g</sup>    | 44 (50.0)                     | 30 (44.8)                   | 21 (65.6)                   | 6 (60.0)                    | 26 (63.4)                     | 127 (53.4)   | 0.194               |
| MMSE <sup>h</sup>              | 21.45 ± 5.64 <sup>c,d</sup>   | 21.49 ± 5.61                | 20.85 ± 5.80 <sup>c</sup>   | 24.04 ± 5.78 <sup>e,f</sup> | 23.88 ± 4.50 <sup>e</sup>     | 22.01 ± 5.56 | 0.003               |
| Tau-PET tracer <sup>g</sup>    |                               |                             |                             |                             |                               |              | <0.001 <sup>i</sup> |
| <sup>18</sup> F-flortaucipir   | 96 (69.1)                     | 73 (70.9)                   | 15 (42.9)                   | 18 (41.9)                   | 18 (26.5)                     | 220 (56.7)   |                     |
| <sup>18</sup> F-MK6240         | 25 (18.0)                     | 18 (17.5)                   | 18 (51.4)                   | 0 (0.0)                     | 29 (42.6)                     | 90 (23.2)    |                     |
| <sup>18</sup> F-PI2620         | 12 (8.6)                      | 7 (6.8)                     | 0 (0.0)                     | 24 (55.8)                   | 21 (30.9)                     | 64 (16.5)    |                     |
| <sup>18</sup> F-RO948          | 6 (4.3)                       | 5 (4.9)                     | 2 (5.7)                     | 1 (2.3)                     | 0 (0.0)                       | 14 (3.6)     |                     |

Values are mean ± standard deviation for continuous variables and n (%) for categorical variables. Differences between groups were assessed using ANOVA, chi-squared tests of independence or the Kruskal-Wallis test. In the case of cell counts <5, Monte Carlo simulations with 20 000 replications (B = 20 000) were employed to estimate the P-values for the chi-squared tests. If a statistically significant main effect was observed, Tukey's Honestly Significant Difference (HSD) test was used as a post hoc test following ANOVA, Fisher's exact tests following chi-square tests, and Dunn's test following the Kruskal-Wallis test. Fisher's exact tests and Dunn's test were adjusted for multiple comparisons using the Bonferroni correction. When data was missing for a category (education n = 89, APOEε4 status n = 150, MMSE n = 79), individuals were excluded from that specific analysis. AD = Alzheimer's disease; APOE = apolipoprotein E; bvAD = behavioural variant Alzheimer's disease; CBS = corticobasal syndrome; lvPPA = logopenic variant primary progressive aphasia; MMSE = mini-mental state examination; PCA = posterior cortical atrophy.

<sup>a</sup>Differences between groups were assessed using ANOVA.

<sup>b</sup>Significantly different from lvPPA-AD.

<sup>c</sup>Significantly different from CBS-AD.

<sup>d</sup>Significantly different from typical AD.

<sup>e</sup>Significantly different from PCA-AD.

<sup>f</sup>Significantly different from bvAD.

<sup>g</sup>Differences between groups were assessed using chi-squared tests of independence.

<sup>h</sup>Differences between groups were assessed using the Kruskal-Wallis test.

<sup>i</sup>All group comparisons were significant, except for PCA-AD versus lvPPA-AD.

**Table 2 Post-mortem cohort: demographic, clinical and neuropathological information across atypical AD variants per site**

|                     | UPENN        |              |               |              | UCSF          |              |              |              |
|---------------------|--------------|--------------|---------------|--------------|---------------|--------------|--------------|--------------|
|                     | PCA-AD       | lvPPA-AD     | bvAD          | CBS-AD       | PCA-AD        | lvPPA-AD     | bvAD         | CBS-AD       |
| N                   | 12           | 23           | 13            | 15           | 7             | 9            | 10           | 4            |
| Age at death, years | 68.08 ± 8.97 | 69.26 ± 7.92 | 74.00 ± 10.88 | 65.87 ± 7.46 | 63.29 ± 3.64  | 66.56 ± 5.81 | 63.50 ± 6.98 | 74.75 ± 9.25 |
| Female              | 3 (25.0)     | 10 (43.5)    | 5 (38.5)      | 11 (73.3)    | 6 (85.7)      | 6 (66.7)     | 2 (20.0)     | 2 (50.0)     |
| Education, years    | 15.83 ± 3.10 | 16.82 ± 2.79 | 15.00 ± 3.11  | 15.14 ± 2.41 | 15.43 ± 2.15  | 14.89 ± 1.96 | 16.12 ± 2.75 | 18.00 ± 6.32 |
| MMSE                | 13.42 ± 8.58 | 9.81 ± 7.53  | 13.73 ± 8.30  | 9.14 ± 4.79  | 12.17 ± 12.42 | 7.22 ± 5.49  | 13.11 ± 6.79 | 19.75 ± 9.50 |
| A (Aβ plaques)      |              |              |               |              |               |              |              |              |
| 2                   | 0 (0.0)      | 0 (0.0)      | 0 (0.0)       | 1 (6.7)      | 0 (0.0)       | 0 (0.0)      | 0 (0.0)      | 1 (25.0)     |
| 3                   | 12 (100.0)   | 23 (100.0)   | 13 (100.0)    | 14 (93.3)    | 4 (100.0)     | 7 (100.0)    | 9 (100.0)    | 3 (75.0)     |
| B (NFTs)            |              |              |               |              |               |              |              |              |
| 2                   | 0 (0.0)      | 0 (0.0)      | 0 (0.0)       | 1 (6.7)      | 0 (0.0)       | 0 (0.0)      | 0 (0.0)      | 1 (25.0)     |
| 3                   | 12 (100.0)   | 23 (100.0)   | 13 (100.0)    | 14 (93.3)    | 7 (100.0)     | 9 (100.0)    | 10 (100.0)   | 3 (75.0)     |
| C (NPs)             |              |              |               |              |               |              |              |              |
| 2                   | 2 (16.7)     | 0 (0.0)      | 2 (15.4)      | 2 (13.3)     | 0 (0.0)       | 0 (0.0)      | 0 (0.0)      | 0 (0.0)      |
| 3                   | 10 (83.3)    | 23 (100.0)   | 11 (84.6)     | 13 (86.7)    | 7 (100.0)     | 9 (100.0)    | 10 (100.0)   | 4 (100.0)    |

Values are mean ± standard deviation for continuous variables and n (%) for categorical variables. Aβ plaques, NFTs and NPs are presented according to ABC-score criteria (A = Aβ plaques using the Thal phase system; B = NFTs using the Braak staging system; C = NPs based on the CERAD criteria).<sup>118</sup> N = 4 missing for education (n = 2 UPENN, n = 2 UCSF), n = 7 for MMSE (n = 5 UPENN, n = 2 UCSF), n = 6 for A (Aβ plaques; all UCSF). Aβ = amyloid-β; AD = Alzheimer's disease; bvAD = behavioural variant Alzheimer's disease; CBS = corticobasal syndrome; lvPPA = logopenic variant primary progressive aphasia; MMSE = mini-mental state examination; NFTs = neurofibrillary tangles; NPs = neuritic plaques; PCA = posterior cortical atrophy; UCSF = university of California, San Francisco; UPENN = university of Pennsylvania.

cohort and the average of subsets of the data derived by systematically excluding one site at a time (i.e. a leave-one-site-out approach) were near perfect across all AD variants (Supplementary Fig. 2). In addition, Levene's test showed that there were no variance differences across all leave-one-site-out scenarios (all  $P > 0.05$ ; see Supplementary Table 2). These findings support the robustness of our results and demonstrate the validity of the tau positivity probability approach, prompting us to continue using it in our main (group-level) analyses.

## Regions with stronger functional connectivity exhibit greater in vivo and post-mortem tau covariance

Our second objective was to test whether higher inter-regional functional connectivity is associated with higher covariance in cross-sectional tau-PET uptake and post-mortem tau pathology. To investigate this, we first explored the association between

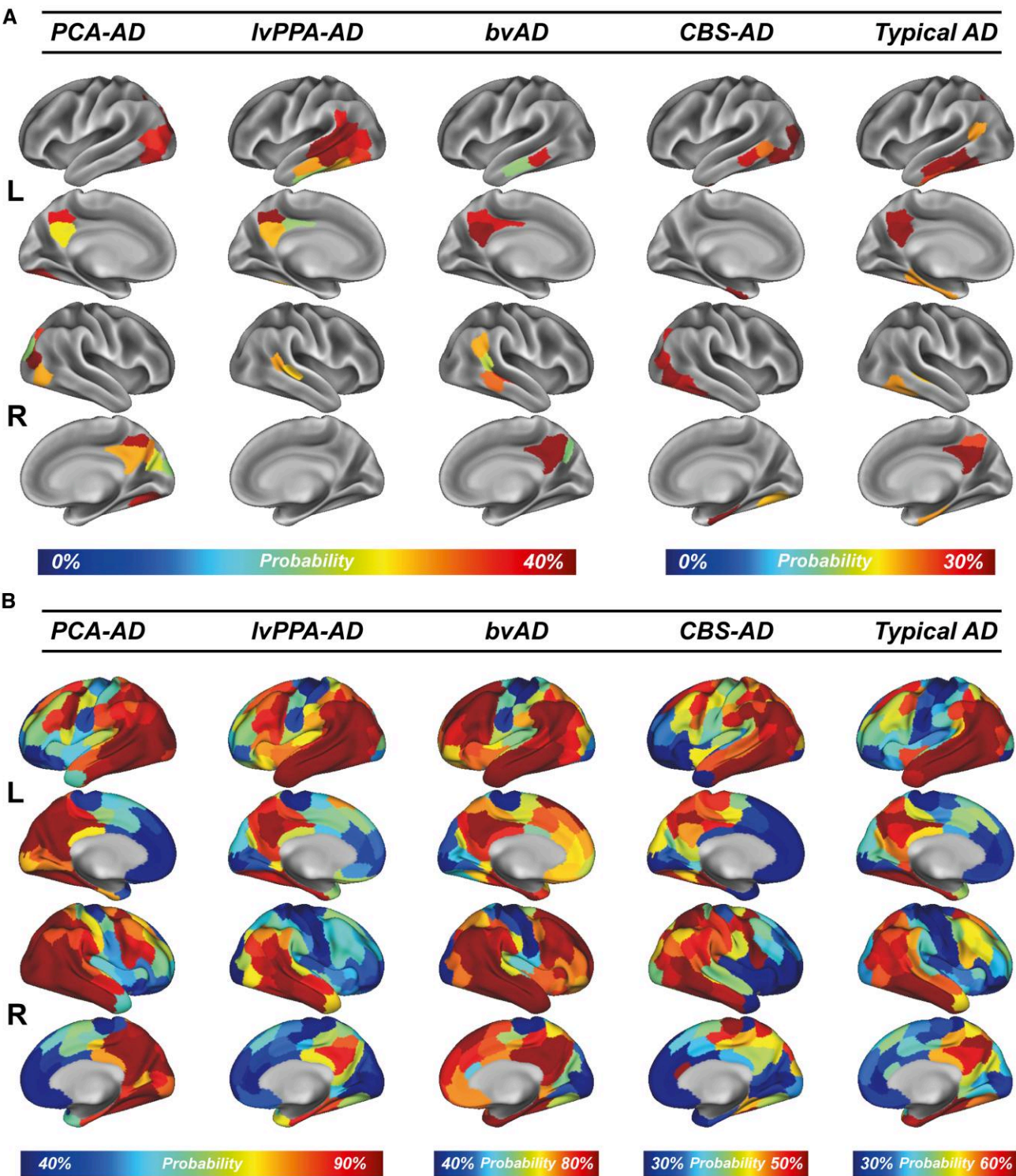


**Figure 1** Tau-PET epicentres and positivity across AD variants. Tau epicentres (i.e. the regions with the assumed earliest and greatest tau burden) were defined at the subject level as the 5% regions with the highest tau-PET SUVRs at baseline. Group-average epicentre probabilities (A) indicate the likelihood of a region being part of the epicentre, with only epicentre probabilities  $\geq 20\%$  shown. Group-average baseline tau-PET positivity probabilities (a uniform tau-PET scale ranging from 0% to 100%) across AD variants are shown in (B). AD = Alzheimer’s disease; bvAD = behavioural variant Alzheimer’s disease; CBS = corticobasal syndrome; L = left; lvPPA = logopenic variant primary progressive aphasia; PCA = posterior cortical atrophy; R = right; SUVR = standardized uptake value ratio.

inter-regional functional connectivity-based distance and inter-regional covariance in tau-PET through linear regression. In all AD variants, analysed separately, greater AD variant-average tau-PET covariance was associated with shorter functional connectivity-based distance. We observed this relationship when assessing connectivity and tau covariance across the whole brain (Fig. 2C–H, PCA-AD:  $\beta = -0.53$ ,  $P < 0.001$ , lvPPA-AD:  $\beta = -0.51$ ,  $P < 0.001$ , bvAD:  $\beta = -0.37$ ,  $P < 0.001$ , CBS-AD:  $\beta = -0.52$ ,  $P < 0.001$ ,



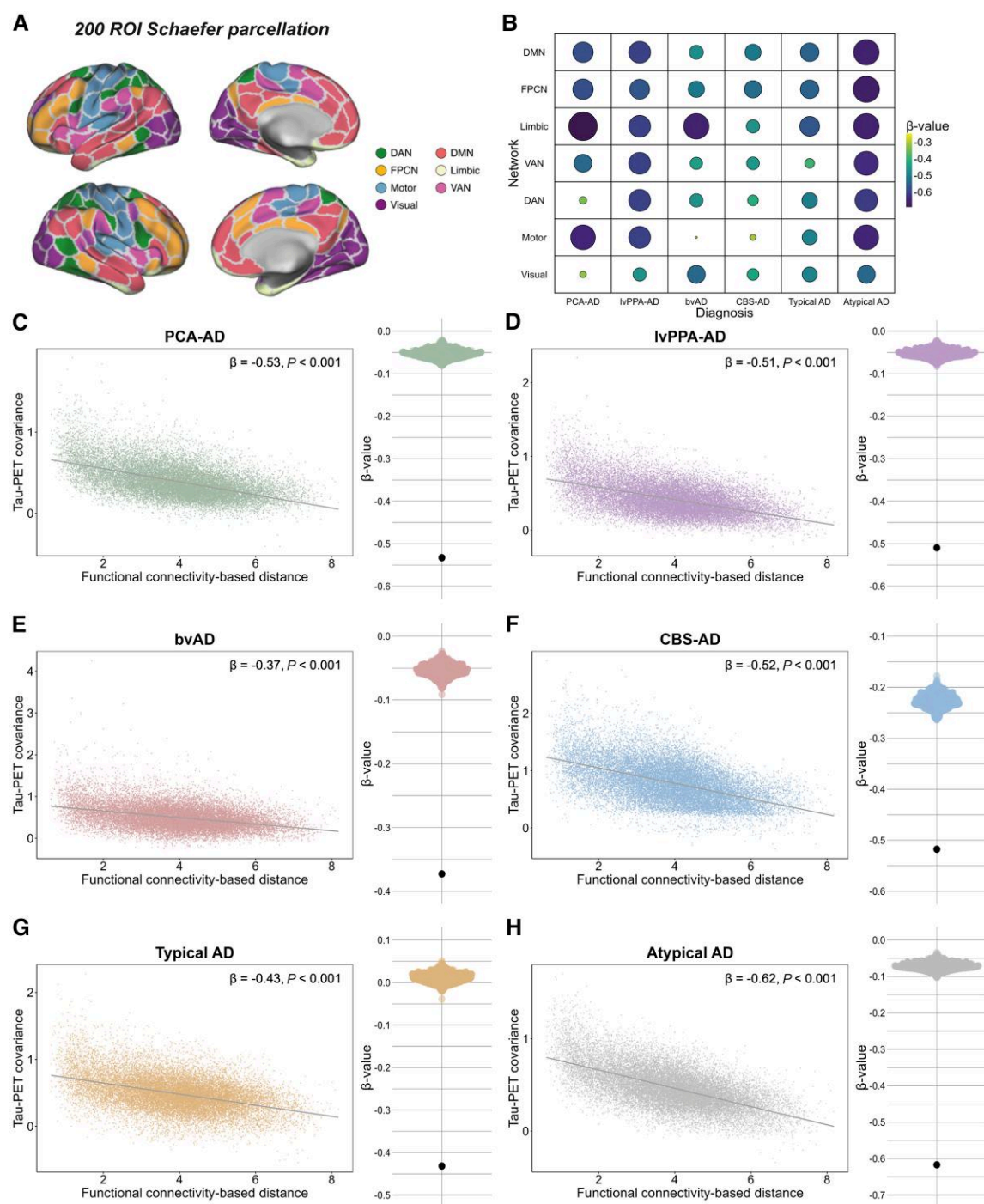


**Figure 2 Association between functional connectivity and covariance in tau-PET across variants of AD.** Surface rendering of the 200 ROI brain atlas used for tau-PET and resting-state functional MRI (fMRI) data in ROI-based analyses (A). Functional connectivity was defined as Fisher z-transformed Pearson correlations between fluctuations in the BOLD signal of all possible 200 Schaefer ROI pairs in 42 CN A $\beta$ -negative individuals from ADNI. The 200  $\times$  200 ROI functional connectivity matrix was density thresholded at 30% (i.e. 30% of the strongest positive connections were retained) and transformed to functional connectivity-based distance (strongly connected regions are 'close', while weakly or indirectly connected regions are 'distant'). Tau-PET covariance was defined as AD variant-average Fisher z-transformed partial Pearson correlations between tau positivity probabilities of all possible ROI pairs, while adjusting for age, sex and site. The association between inter-regional functional connectivity-based distance and inter-regional tau-PET covariance was assessed using linear regression for all AD variants, both across the whole brain (C–H) and in seven individual resting-state fMRI networks separately (A and B). To test the robustness of these findings, we re-ran the whole-brain analysis 1000 times, each time using a different connectivity null model from the set of 1000 null models that were generated by shuffling the connectivity matrix while preserving the weight and degree distribution. This procedure resulted in a distribution of  $\beta$ -values based on the null models, as depicted in the beeswarm panels in C–H, where the actual  $\beta$ -value (furthest data-point) always exceeded the null model  $\beta$ -values. A $\beta$  = amyloid- $\beta$ ; AD = Alzheimer's disease; ADNI = Alzheimer's disease neuroimaging initiative; BOLD = blood oxygen level-dependent; bvAD = behavioural variant Alzheimer's disease; CBS = corticobasal syndrome; CN = cognitively normal; DAN = dorsal attention network; DMN = default mode network; FPCN = frontoparietal control network; lvPPA = logopenic variant primary progressive aphasia; PCA = posterior cortical atrophy; ROI = region of interest; VAN = ventral attention network.

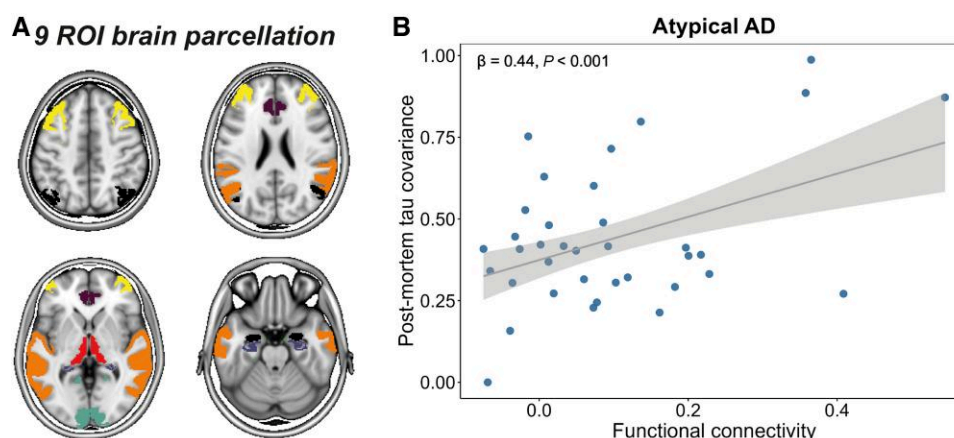


**Figure 3 Association between functional connectivity and covariance in post-mortem tau pathology in atypical AD.** Using established cortical and sub-cortical brain atlases (i.e. AAL, CoBrA, Julich, Neuromorphometrics), we created a bilateral MRI brain atlas for the regions with post-mortem tau assessment ( $n = 9$ , see A). Functional connectivity was defined as Fisher z-transformed Pearson correlations between functional MRI (fMRI) time series (reflective of fluctuations in the BOLD signal) of all ROI pairs in 42 CN A $\beta$ -negative individuals from ADNI. Tau covariance was defined as Fisher z-transformed partial Spearman correlations between semi-quantitative tau pathology ratings of all ROI pairs, while adjusting for age and sex. We pooled the data from all AD variants to increase statistical power. The association between inter-regional functional connectivity and inter-regional tau pathology covariance was assessed using linear regression (B). AAL = automated anatomical labelling; A $\beta$  = amyloid- $\beta$ ; AD = Alzheimer's disease; ADNI = Alzheimer's disease neuroimaging initiative; BOLD = blood oxygen level-dependent; CN = cognitively normal; CoBrA = computational brain anatomy laboratory; ROI = region of interest.

typical AD:  $\beta = -0.43$ ,  $P < 0.001$ , atypical AD altogether:  $\beta = -0.62$ ,  $P < 0.001$ ), as well as within seven individual functional brain networks (Fig. 2 A and B and Supplementary Fig. 3), suggesting that the association between connectivity and covariance in tau is not confined to specific high-tau regions. The results remained consistent when adjusting for inter-regional Euclidean distance (Supplementary Fig. 4), suggesting that functional connectivity (and not spatial proximity) is the main driver of these associations. To test the robustness of these findings, we performed a previously described bootstrapping procedure in which 1000 connectivity null models were generated by shuffling the  $200 \times 200$  connectivity matrix while preserving the weight and degree distribution.<sup>8</sup> Subsequently, we re-ran the whole-brain linear model 1000 times, each time using a different connectivity matrix, which resulted in a distribution of null-model  $\beta$ -values (Fig. 2C–H). We then compared the actual  $\beta$ -value from the observed true connectivity matrix to the  $\beta$ -values generated by the null models using exact tests. This enabled us to determine the frequency with which the  $\beta$ -values from the null models exceeded the actual  $\beta$ -value. For all AD variants, the null model  $\beta$ -values never exceeded the actual  $\beta$ -value, further strengthening our findings.

In addition to the tau-PET analyses, we also examined the relationship between functional connectivity and tau covariance using post-mortem data. Given that the tau-PET signal can be confounded by factors other than tau pathology, such as binding to off-target sources like astrogliosis or iron accumulation,<sup>76,77</sup> the reliability of the tau-PET findings would be strengthened by post-mortem replication. We assessed the association between inter-regional functional connectivity [i.e. a matrix with Fisher z-transformed Pearson correlations between the fMRI time series of all ROI pairs (using ADNI elderly control data)] and inter-regional post-mortem tau covariance [i.e. Fisher z-transformed age- and sex-adjusted partial Spearman (in the semi-quantitative UPENN dataset) or Pearson (in the quantitative UCSF dataset) correlations between tau pathology ratings of all ROI pairs] using linear

regression. For this analysis, we pooled data from all atypical AD variants to increase statistical power. Consistent with our hypothesis and previous tau-PET results, UPENN data ( $n = 63$ ) showed that stronger functional connectivity was associated with higher covariance in post-mortem tau pathology across nine ROIs,  $\beta = 0.44$ ,  $P < 0.001$  (Fig. 3). Although the analysis did not reach statistical significance, the direction of this effect was confirmed in the smaller UCSF replication sample ( $n = 30$ ),  $\beta = 0.36$ ,  $P = 0.116$  (Supplementary Fig. 5).

### Regions more functionally connected to the tau-PET epicentre show higher tau-PET levels

Our third objective was to test the hypothesis that functional connectivity of specific tau-PET epicentres is associated with tau progression sequences inferred from cross-sectional data. For each AD variant separately, we used linear regression to test the association between epicentre connectivity and tau-PET levels. Our findings showed that, across all AD variants, a shorter functional connectivity-based distance to the tau epicentre was associated with higher tau-PET SUVRs, both when tested at the subject level (Fig. 4A–E) and per tracer at the group level (Supplementary Fig. 6). To further investigate this, we divided all brain regions (excluding the epicentre) into quartiles based on their functional proximity to the tau epicentre. We then examined whether regions in the lower quartiles (i.e. regions functionally most strongly connected to the tau epicentre) had higher tau positivity probabilities than those in the higher quartiles (i.e. regions functionally distant from the tau epicentre). As expected, a gradient of increasing tau positivity probabilities was observed from quartile 4 to quartile 1 across all AD variants (Fig. 4A–E; paired Wilcoxon signed-rank tests indicating  $P < 0.05$  for all quartile comparisons). When repeating these analyses in a subset of individuals with subject-level fMRI available (PCA-AD  $n = 6$ , lvPPA-AD  $n = 5$ , CBS-AD  $n = 5$ ), the results were generally comparable to the main analyses (Supplementary Fig. 7). Paired Wilcoxon signed-rank tests for the entire atypical AD group were significant ( $P < 0.05$ ) for all quartile comparisons,

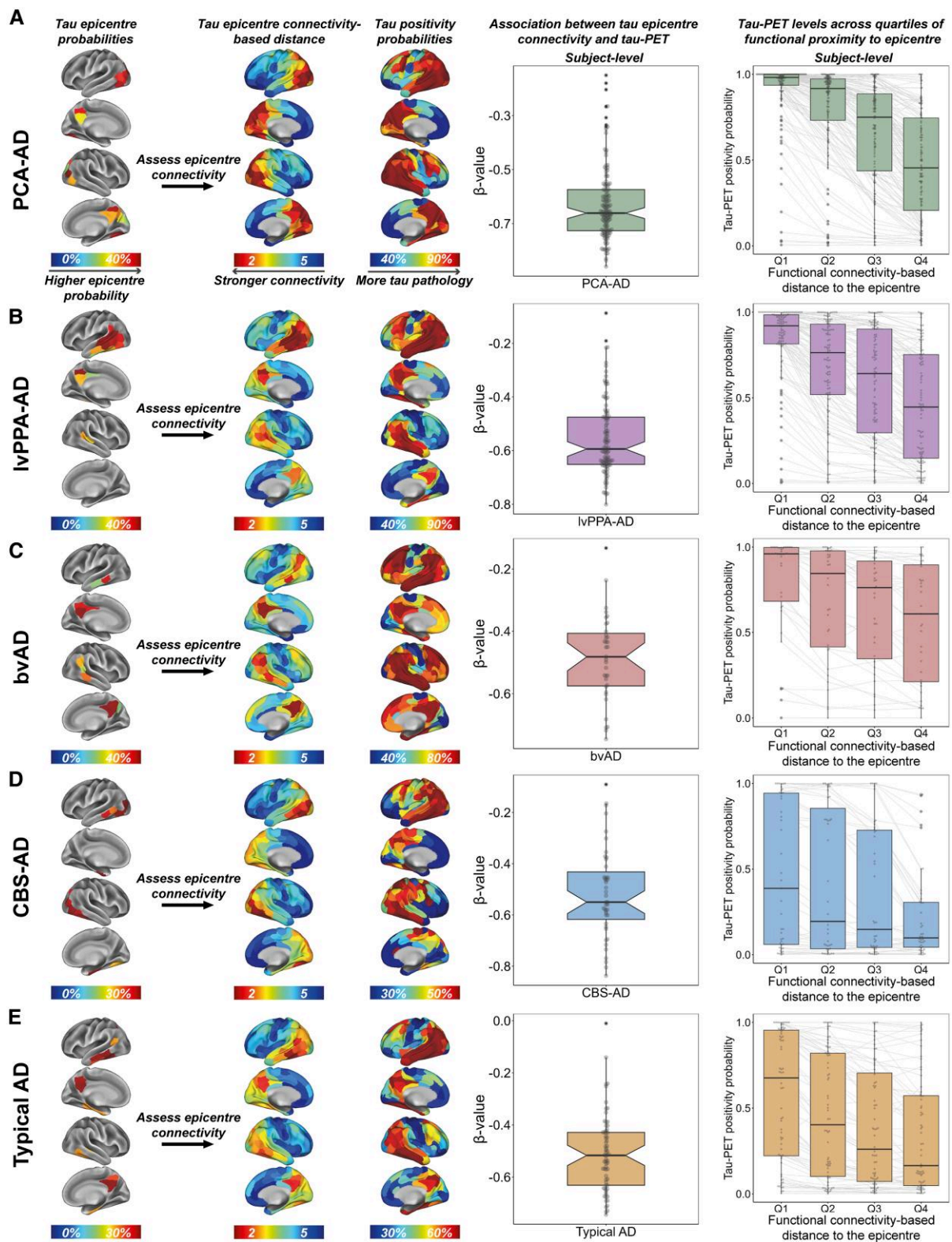


**Figure 4** Association between tau epicentre connectivity and tau-PET across AD variants. Tau epicentre connectivity was determined by taking the functional connectivity-based distance (see Fig. 2 for method specifications) of each non-epicentre ROI ( $n = 190$ ) to the epicentre ( $n = 10$ ). For each individual, linear regression was used to assess the association between functional connectivity-based distance to the tau epicentre and tau-PET SUVR. Subject-level  $\beta$ -values are visualized per AD variant in the notched boxplots in A–E. Additionally, all non-epicentre regions were grouped into quartiles based on their functional proximity to the epicentre (quartile 1 = shortest functional connectivity-based distance, quartile 4 = longest functional connectivity-based distance), and tau positivity probabilities across quartiles were compared using paired Wilcoxon signed-rank tests. AD = Alzheimer's disease; bvAD = behavioural variant Alzheimer's disease; CBS = corticobasal syndrome; IvPPA = logopenic variant primary progressive aphasia; PCA = posterior cortical atrophy; Q = quartile; ROI = region of interest; SUVR = standardized uptake value ratio.



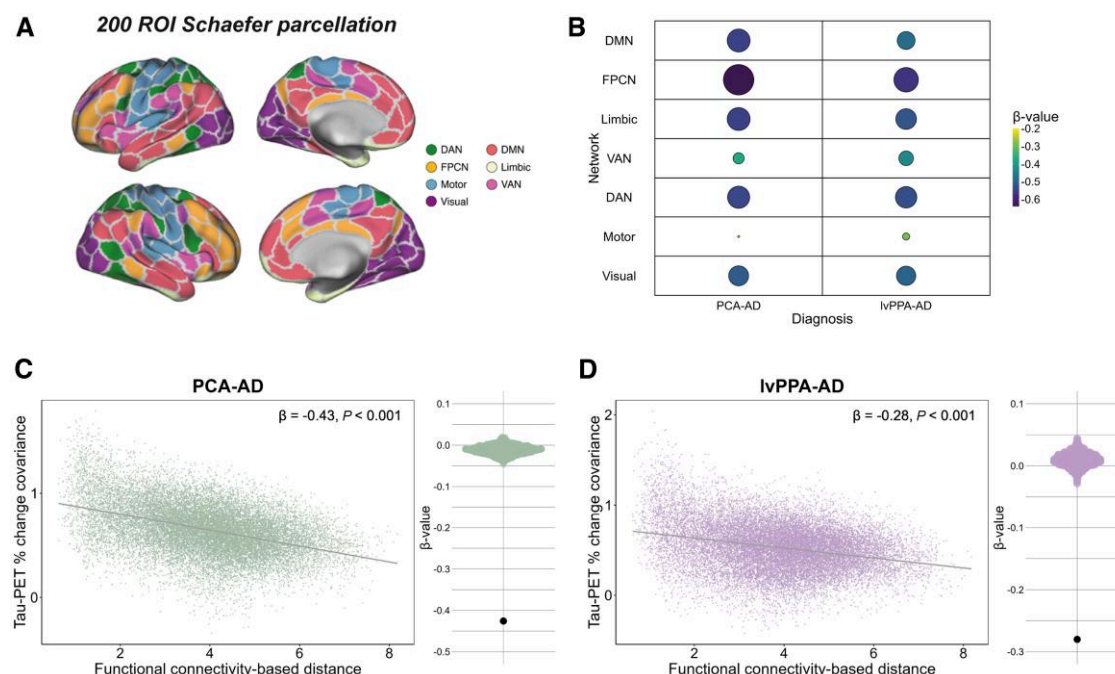


**Figure 5 Association between functional connectivity and covariance in tau-PET percentage change in PCA-AD and lvPPA-AD.** Surface rendering of the 200 ROI brain atlas used for tau-PET and resting-state functional MRI (fMRI) data in ROI-based analyses (A). We computed annual tau-PET SUVR change for each individual by fitting 200 linear models (one for each ROI), using follow-up time as the independent variable and tau-PET SUVR as the dependent variable. We then normalized each ROI's rate of change by the individual's initial SUVR (at follow-up time = 0) to express it as a relative percentage change per year. Covariance in tau-PET percentage change was determined by calculating AD variant-average Fisher z-transformed partial Pearson correlations between the percentage change rates of all ROI pairs while adjusting for age, sex and site. Using the functional connectivity-based distance matrix described in Fig. 2, we assessed the association between inter-regional functional connectivity-based distance and inter-regional tau-PET percentage change covariance through linear regression, both across the whole brain (C and D) and in seven individual resting-state fMRI networks separately (A and B). We re-ran the analysis 1000 times (same procedure as described in Fig. 2) to test the robustness of our findings, as illustrated in the beeswarm panels in C and D, where the actual  $\beta$ -value (furthest data-point) always exceeded the null model  $\beta$ -values. AD = Alzheimer's disease; DAN = dorsal attention network; DMN = default mode network; FPCN = frontoparietal control network; lvPPA = logopenic variant primary progressive aphasia; PCA = posterior cortical atrophy; ROI = region of interest; SUVR = standardized uptake value ratio; VAN = ventral attention network.

except for quartile 2 versus quartile 3, which was borderline significant ( $P = 0.07$ ). These analyses support our hypothesis that tau progression across the brain follows the pattern of functional connections from the tau epicentre, across atypical AD variants.

### Regions with stronger functional connectivity exhibit greater covariance in tau-PET change

Our fourth objective was to test whether higher inter-regional functional connectivity is associated with higher covariance in tau-PET accumulation rates over time. Due to the relatively small sample sizes in the other groups, we only included the PCA-AD and lvPPA-AD groups for our longitudinal analyses. We investigated the association between functional connectivity-based distance across 200 ROIs (as described before) and inter-regional covariance in longitudinal tau-PET change through linear regression. In both PCA-AD and lvPPA-AD, we observed that greater covariance in tau-PET percentage change was associated with shorter functional connectivity-based distance, both across the whole brain (Fig. 5C and D; PCA-AD:  $\beta = -0.43, P < 0.001$ , lvPPA-AD:  $\beta = -0.28, P < 0.001$ ) and in seven individual resting-state fMRI networks (Fig. 5A and B and Supplementary Fig. 8). When we re-ran the whole-brain analyses 1000 times to test the robustness of our findings, we found that none of the null model-derived  $\beta$ -values exceeded the actual  $\beta$ -value (Fig. 5C and D). These results indicate that regions with

stronger functional connectivity to each other show greater congruence in tau-PET change over time.

### Regions more functionally connected to the tau-PET accumulation epicentre show faster tau-PET change

Our fifth objective was to establish whether functional connectivity of tau-PET accumulation epicentres predicts faster longitudinal increases in tau. We thus aimed to evaluate whether brain regions in closer functional proximity to the tau-PET accumulation epicentre exhibited more tau-PET change than functionally more remote regions. Therefore, we first determined the tau-PET accumulation epicentre for each individual, i.e. the top 5% of regions exhibiting the highest annual tau-PET SUVR percentage change. Then, for PCA-AD and lvPPA-AD separately, we used linear regression to assess the association between subject-level tau accumulation epicentre connectivity and tau-PET percentage change over time. Our results revealed that tau accumulation predominantly occurred anteriorly in PCA-AD (Fig. 6A). Moreover, in lvPPA-AD it was primarily observed in right temporoparietal and occipital regions (Fig. 6B), which likely reflects the close functional connectivity of these regions to the baseline tau-PET epicentres of both variants.<sup>14,51,78</sup> Moreover, for both PCA-AD and lvPPA-AD, a shorter functional connectivity-based distance to the tau accumulation epicentre was associated with faster tau-PET change, both when tested at the subject level (Fig. 6A and B) and per tracer at the group

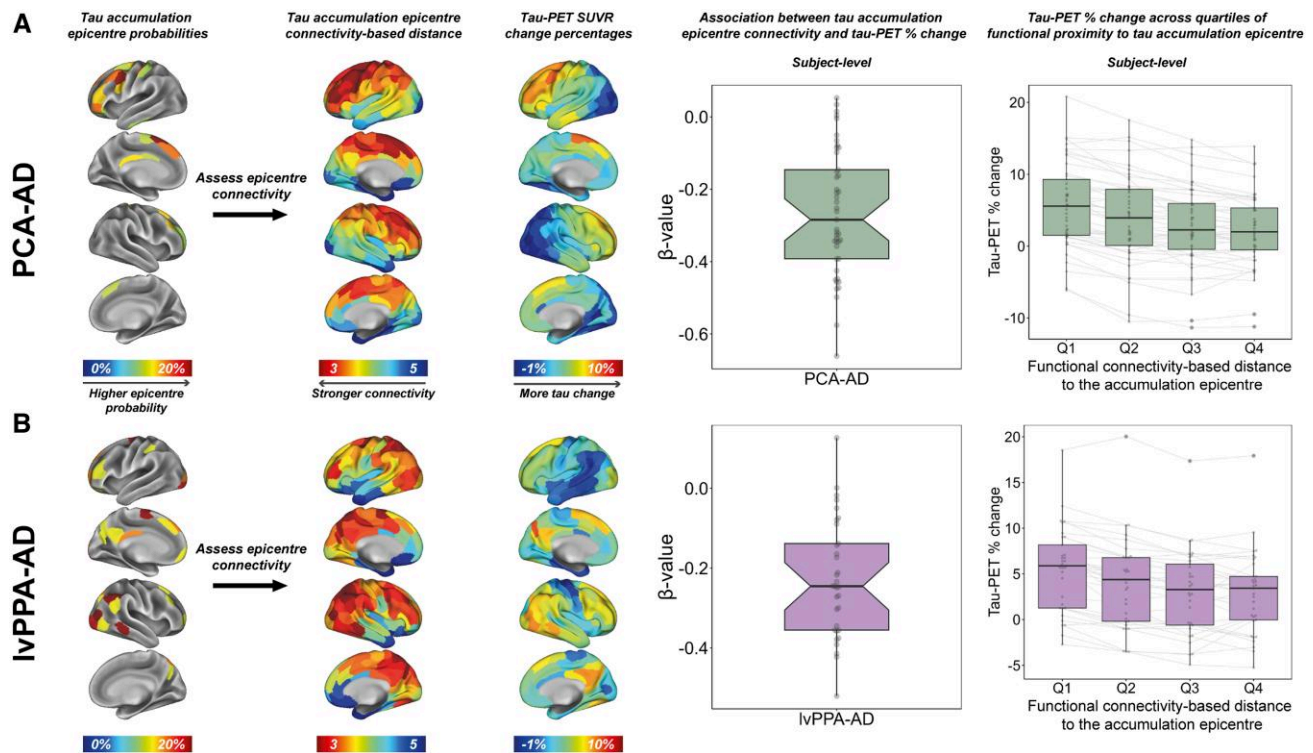


**Figure 6** Association between tau accumulation epicentre connectivity and tau-PET change in PCA-AD and lvPPA-AD. Tau accumulation epicentres were defined as the top 5% of ROIs (i.e. 10 ROIs in total) with the highest annual percentage change in tau-PET SUVR. Group-average epicentre probabilities indicate the likelihood of a region being part of the epicentre, with only epicentre probabilities  $\geq 10\%$  shown. Tau accumulation epicentre connectivity was determined by taking the functional connectivity-based distance (see Fig. 2 for method specifications) of each non-accumulation-epicentre ROI ( $n = 190$ ) to the accumulation epicentre ( $n = 10$ ). For each individual, linear regression was used to assess the association between functional connectivity-based distance to the tau accumulation epicentre and tau-PET annual percentage change. Subject-level  $\beta$ -values are visualized per AD variant in the notched boxplots in A and B. Additionally, all non-accumulation-epicentre regions were grouped into quartiles based on their functional proximity to the accumulation epicentre (quartile 1 = shortest functional connectivity-based distance, quartile 4 = longest functional connectivity-based distance), and tau-PET percentage change rates across quartiles were compared using paired Wilcoxon signed-rank tests. AD = Alzheimer's disease; lvPPA = logopenic variant primary progressive aphasia; PCA = posterior cortical atrophy; Q = quartile; ROI = region of interest; SUVR = standardized uptake value ratio.

level (Supplementary Fig. 9). We again divided all brain regions (excluding the tau accumulation epicentre) into quartiles based on their functional proximity to the accumulation epicentre. We then examined whether regions in the lower quartiles (i.e. regions functionally close) showed more tau-PET change than those in the higher quartiles (i.e. regions functionally distant). A gradient of increasing tau-PET change was observed from quartile 4 to quartile 1 for both variants (Fig. 6A and B). Paired Wilcoxon signed-rank tests showed significance ( $P < 0.05$ ) for all quartile comparisons, except for quartile 3 versus quartile 4 in lvPPA-AD. These analyses support our hypothesis that tau propagates across the brain along functional connections, not only in typical AD but also consistently across atypical AD variants with highly heterogeneous tau deposition patterns.

## Discussion

The primary aim of this study was to determine whether connectivity serves as a universal scaffold for predicting tau progression in AD, independent of clinical phenotype or regional predilection of tau deposition. To this end, we conducted a multicentre study combining tau-PET ( $n = 320$  cross-sectional,  $n = 78$  longitudinal) and post-mortem ( $n = 93$ ) data across 14 sites from various atypical AD variants (i.e. PCA-AD, lvPPA-AD, bvAD and CBS-AD). In line with

our primary hypothesis, we found that in all AD variants, brain regions with stronger functional connectivity to each other exhibited greater covariance in concurrent tau-PET deposition and tau-PET change over time. Importantly, this finding was replicated using regionally sampled post-mortem data, wherein we observed that stronger functional connectivity was associated with higher covariance in tau. Furthermore, across all AD variants, brain regions with stronger functional connectivity to the tau-PET epicentre (i.e. the top 5% of regions with the highest tau-PET retention) showed higher tau-PET levels at baseline. Similarly, regions with stronger functional connectivity to the tau-PET accumulation epicentre (i.e. the top 5% of regions with the highest tau accumulation over time) demonstrated faster rates of longitudinal tau-PET accumulation. Taken together, these findings support the hypothesis that tau progresses throughout the brain along functional connections, although spatial progression may also reflect shared vulnerability of connected regions to activity-dependent stressors and proteostasis.<sup>28</sup> Importantly, connectivity-related progression seems to be consistent across AD phenotypes, establishing functional connectivity as a universal framework for tau progression and highlighting the heightened vulnerability of highly connected brain networks to tau pathology in AD.<sup>79</sup>

Our finding that strongly functionally connected brain regions show correlated tau levels and tau accumulation, and that the

functional connectivity of tau epicentres predicts tau progression, aligns with previous studies suggesting that tau pathology propagates through the brain in a prion-like manner, spreading along synaptic connections from cell to cell.<sup>10,12,80,81</sup> While functional connectivity reflects coordinated activity between brain regions, it is also related to structural connectivity, which can be assessed by methods like diffusion tensor imaging (DTI).<sup>82</sup> DTI, despite the limitation to accurately capture U-fibres and crossing fibres, reflects anatomical links between areas.<sup>8,82</sup> Structurally connected regions often show strong functional connectivity, as direct physical pathways facilitate efficient communication.<sup>82</sup> These structural connections likely serve as routes for the trans-synaptic spread of tau pathology, with both functional and structural networks jointly explaining the observed spatiotemporal patterns of tau accumulation.<sup>15</sup> Examples of trans-neuronal tau spread have been demonstrated in cellular models of tauopathy, where tau aggregates, or ‘seeds,’ can be released from donor cells, subsequently taken up by recipient cells and then trigger the aggregation of normally soluble tau.<sup>9,22,23,83–88</sup> This transcellular transfer mechanism is also observed in transgenic or supraphysiological animal models, where tau injections into specific brain regions lead to the emergence of tau pathology in connected areas, reinforcing the concept of network-based propagation.<sup>11,24–26,89–97</sup> Recent human neuroimaging studies align with these preclinical findings, showing that tau pathology progresses from localized epicentres—proposed to harbour the earliest and highest levels of tau—to connected brain regions.<sup>5,7,13,16–21,27,98</sup> However, these studies have primarily shown that brain connectivity predicts tau progression in typical amnesic AD, where tau follows the stereotypical Braak staging scheme.<sup>1</sup> To address this limitation, we included atypical AD variants, each of which display unique tau deposition patterns.<sup>40</sup> By doing so, our findings provide novel insights into the mechanisms of tau pathology, showing that tau progresses along functional brain connections—also in atypical AD. This supports the universality of network-based tau progression across diverse AD phenotypes and offers a broader framework for understanding tau propagation in complex and less predictable cases of AD.

An unexpected finding was the predominance of tau pathology in the posterior and temporal cortices in the CBS-AD group, contrasting with previous studies that showed significant involvement of the sensorimotor cortex.<sup>40,42</sup> However, compared with the other AD variants, CBS-AD exhibited greater tau burden in the sensorimotor cortex, suggesting that it was relatively more affected in CBS-AD despite prominent tau accumulation in classical AD regions. This became even more evident when stratifying by lateralization of the clinical symptoms, as subgroup analyses revealed subtle asymmetric tau deposition, with greater tau accumulation in the sensorimotor cortex contralateral to the clinically affected body side. Moreover, since CBS-AD is not limited to motor symptoms, the posterior tau pathology may underlie other clinical features commonly seen in CBS-AD, such as apraxia or visuospatial deficits.<sup>38</sup>

Given that tau is a key driver of neurodegeneration and cognitive decline in AD,<sup>2–4</sup> our findings have significant implications for personalized medicine and clinical trial design. Understanding the mechanisms and patterns of tau propagation can refine both the timing and application of anti-tau therapies. Predicting which brain regions are most vulnerable to tau spread could enable earlier interventions to halt the cascade of neurodegeneration before critical brain areas are affected. In clinical settings, advanced imaging and computational modelling could be used to identify these at-risk regions, allowing clinicians to anticipate the trajectory of tau

spread and strategically time interventions. Administering anti-tau therapies before the pathology compromises key brain areas could help preserve cognitive function and slow disease progression. These insights are particularly relevant for clinical trials, where addressing the heterogeneity across AD variants is a major challenge. Since different AD phenotypes show distinct patterns of tau pathology,<sup>5,16,20,39–43</sup> our findings support the use of individualized ROIs rather than one-size-fits-all approaches when tau-PET is used as an outcome measure.<sup>99</sup> Patient-specific ROIs tailored to functional connectivity and tau pathology patterns could improve trial sensitivity, enhance the detection of treatment effects and ultimately increase the likelihood of successful therapeutic outcomes. While tau-PET is not yet widely available in clinical practice, these findings suggest that it may, in the future, play a role in identifying vulnerable brain regions and monitoring disease progression in the clinic.<sup>100,101</sup> Combined with functional connectivity measures, tau-PET could provide a valuable tool for guiding clinical decision-making and improving patient care.

A major strength of this study is its large sample size with relatively rare AD phenotypes, recruited from 14 sites worldwide, with baseline and longitudinal tau-PET data as well as post-mortem tau assessments available. Notably, the additional inclusion of post-mortem tau assessments—a feature not present in a previous study on functional connectivity and tau spread in atypical AD<sup>16</sup>—represents a novel aspect of our work. There are also several limitations. First, the use of different tau-PET tracers, scanning protocols and approaches for determining A $\beta$  status across sites posed harmonization challenges. Also, A $\beta$  status thresholds were cohort-specific. However, given the high general concordance between amyloid-PET and CSF (~90%),<sup>102</sup> we expect limited impact from the use of different methods for determining A $\beta$  status. Second, as expected based on the young age and atypical clinical presentation,<sup>103</sup> most individuals in the cohort showed signs of saturation in tau-PET retention at baseline, which prevented the ability to directly model longitudinal tau progression from cross-sectional epicentres. Instead, we adopted a tau-PET accumulation epicentre approach, identifying regions with the highest accumulation of tau over time and examining whether tau progresses along the functional connections of these epicentres.<sup>8</sup> Third, it is challenging to determine the true origin of tau pathology in the brain (i.e. the epicentre) in symptomatic stages of AD. Although our epicentre approach suggests that regions with the highest tau-PET values are variant-specific in atypical AD, it remains possible that tau initially arises in the medial temporal lobe, as seen in typical AD,<sup>17,104</sup> but spreads to the neocortex much earlier in atypical variants, leading to the observed differences in tau distribution compared with typical AD. Inter-individual differences in brain architecture may promote this; for example, there is evidence that individuals with developmental disorders, where brain connectivity patterns may need to adapt, are at higher risk of atypical AD manifestations.<sup>105–108</sup> This could be because their brain networks predispose them to faster spread from the medial temporal lobe to other regions. Fourth, in the post-mortem part of the study, tau pathology was assessed in only one hemisphere per individual, which may not fully capture lateralized pathology, especially in syndromes like lvPPA-AD and CBS-AD where asymmetric neuropathologic distributions are well documented.<sup>36,38</sup> Fifth, the two sites that provided post-mortem tau data employed different methodologies. Specifically, UPENN used a semi-quantitative approach with PHF-1 staining,<sup>62</sup> while UCSF utilized a quantitative method with thioflavin-S fluorescent microscopy staining.<sup>61</sup> These methods measure distinct aspects of tau pathology: PHF-1 does not



differentiate between tau species and could therefore be hypothesized to be more aligned with tau-PET, while thioflavin-S particularly measures NFTs.<sup>109–111</sup> Sixth, the spatial resolution of PET imaging is limited,<sup>112</sup> which precludes directly investigating trans-synaptic tau spreading. This limitation implies that, even though our findings lend support to preclinical observations from animal and cellular studies, we are unable to make strong mechanistic inferences about tau propagation due to scale differences (macro versus micro) between our experimental design and these preclinical models. In addition, our study offers only indirect evidence for the trans-synaptic tau spreading hypothesis, and alternative mechanisms (e.g. shared regional vulnerability between connected brain regions) may give rise to similar connectivity-dependent patterns of tau progression.<sup>113,114</sup> Seventh, to ensure consistency with our fMRI analyses and effectively capture functional brain networks, we used the cortical Schaefer atlas<sup>58</sup> for our tau-PET analyses. However, this choice prevented us from examining tau-PET in subcortical regions, which may be particularly relevant for CBS-AD, where there could be some subcortical involvement.<sup>75,115,116</sup> Additionally, the high granularity of the 200 ROI atlas may increase the risk of partial volume effects, potentially making regional tau estimates less precise.

In conclusion, the current study provides strong evidence that, in AD, tau progression is predictable according to the brain's functional connections, independent of the clinical phenotype and the topography of tau load. Future research is warranted in several key areas, including: (i) advancing and validating functional connectivity-based models to more accurately predict individual levels of tau progression, ideally utilizing subject-level fMRI, because such mechanistic understanding will be crucial for identifying potential novel drug targets aimed at slowing or preventing tau accumulation; (ii) elucidating the role of A $\beta$  burden in shaping tau progression patterns across AD variants. Although direct examination was not possible due to differences in modalities for defining A $\beta$  status and the use of different amyloid-PET tracers, prior work in e.g. PCA and lvPPA suggests that regional A $\beta$  deposition may influence local tau accumulation.<sup>117,118</sup> Therefore, future studies with harmonized approaches will be critical to clarify this relationship; (iii) investigating interactions between tau and other proteinopathies, such as  $\alpha$ -synuclein and TAR DNA-binding protein 43 (TDP-43), as these co-pathologies may influence tau propagation and regional vulnerability<sup>21,119,120</sup>; and (iv) improving the clinical characterization of atypical AD phenotypes,<sup>46</sup> which could facilitate the recruitment of larger and more well-characterized cohorts and enable more uniform scanning protocols and tau-PET tracers. Collectively, these advancements will refine our understanding of tau dynamics, enhance the translational potential of this research for therapeutic development, inform clinical trial design and eventually aid in improving patient care.

## Data availability

Due to the multicentre design of the study, access to individual participant data from each cohort will have to be made available through the principal investigators of the respective cohorts. Generally, anonymized data can be shared by request from qualified academic investigators for the purpose of replicating procedures and results presented in the article, if data transfer is in agreement with the data protection regulation at the institution and is approved by the local Ethics Review Board.

## Acknowledgements

This manuscript was facilitated by the Alzheimer's Association International Society to Advance Alzheimer's Research and Treatment (ISTAART), through the Atypical Alzheimer's disease professional interest area (PIA). The views and opinions expressed by authors in this publication represent those of the authors and do not necessarily reflect those of the PIA membership, ISTAART or the Alzheimer's Association. We would like to thank all our participant volunteers for their participation in this study, as well as all precursor suppliers for the production of the tracers at the respective sites. H.d.B., C.G., R.O. and N.F. (Amsterdam, Munich) contributed to writing this article. The rest of the co-authors critically reviewed the article. Data used in preparation of this article were obtained from the Alzheimer's Disease Neuroimaging Initiative (ADNI) database (adni.loni.usc.edu). As such, the investigators within the ADNI contributed to the design and implementation of ADNI and/or provided data but did not participate in the analysis or writing of this article. A complete listing of ADNI investigators can be found at: [http://adni.loni.usc.edu/wp-content/uploads/how\\_to\\_apply/ADNI\\_Acknowledgement\\_List.pdf](http://adni.loni.usc.edu/wp-content/uploads/how_to_apply/ADNI_Acknowledgement_List.pdf).

## Funding

The Amsterdam team reports: this project was funded by Alzheimer Nederland (WE.03-2021-12cb) and Alzheimer Forschung Initiative e.V. (21010CB). The Cambridge team reports: the study was co-funded by the Dementias Platform UK and Medical Research Council (MC\_UU\_00030/14; MR/T033371/1); the Wellcome Trust (220258); Race Against Dementia Alzheimer's Research UK (ARUK-RADF2021A-010); NIHR Cambridge Biomedical Research Centre (NIHR203312; the views expressed are those of the authors and not necessarily those of the NIHR or the Department of Health and Social Care) and the UK Dementia Research Institute through UK DRI Ltd, principally funded by the Medical Research Council. The Cologne team reports: German Research Foundation (DFG) #329109473, Alzheimer Forschung Initiative e.V. M.H. and G.B. received funding from the Alzheimer Forschung Initiative e.V. In addition, this study was supported by the German Research Foundation [DFG; DR 445/9-1 (A.D.), CRC1451-C04 Project-ID 431549029 (A.D., G.B.)]. The Leipzig team reports: Life Molecular Imaging CMC. Additionally, they report for MLS (Clinic for Cognitive Neurology/MPi): the German Research Foundation (DFG; SCHR 774/5-1) & eHealthSax Initiative of the Sächsische Aufbaubank (SAB; project TelDem), accordingly, study co-financed with tax revenue based on the budget approved by the Saxon state parliament. The Lund team reports: work at the authors' research centre was supported by the European Research Council (ADG-101096455 and ADG-101053962), Alzheimer's Association (ZEN24-1069572, SG-23-1061717), GHR Foundation, Swedish Research Council (2022-00775, 2021-02219, 2023-00356, 2022-01018, 2019-02397), ERA PerMed (ERAPERMED2021-184), Knut and Alice Wallenberg Foundation (2022-0231), Strategic Research Area MultiPark (Multidisciplinary Research in Parkinson's disease) at Lund University, Swedish Alzheimer Foundation (AF-980907, AF-994229), Swedish Brain Foundation (FO2021-0293, FO2023-0163), WASP and DDLs Joint call for research projects (WASP/DDLS22-066), Parkinson Foundation of Sweden (1412/22), Cure Alzheimer's fund, Rönström Family Foundation, Konung Gustaf V:s och Drottning Victorias Frimurarestiftelse, Skåne University Hospital Foundation (2020-O000028), Regionalt Forskningsstöd (2022-1259) and Swedish federal government under

the ALF agreement (2022-Projekt0080, 2022-Projekt0107, ALFGBG-71320). The precursor of 18F-flutemetamol was sponsored by GE Healthcare. The precursor of 18F-RO948 was provided by Roche. The Mayo team reports: National Institutes of Health, grant/award number: R01-AG50603. The MGH team reports: US National Institutes of Health (R01 DC014296, R01 AG081249, R01 AG085377, RF1 NS131395, K01 AG084820, R21 AG080588, K23 AG065450, K23 DC016912, P50 AG005134, and P30 AG062421) Massachusetts General Hospital (Tommy Rickles Chair in Primary Progressive Aphasia Research). The McGill team reports: the TRIAD cohort is supported by the Weston Brain Institute, Canadian Institutes of Health Research (MOP-11-51-31; RFN 152985, 159815 and 162303), Canadian Consortium of Neurodegeneration and Aging (MOP-11-51-31-team 1), the Alzheimer's Association (NIRG-12-92090 and NIRP-12-259245), Brain Canada Foundation (CFI Project 34874; 33397), the Fonds de Recherche du Québec-Santé (Chercheur Boursier, 2020-VICO-279314) and the Colin J. Adair Charitable Foundation. The Munich team reports: this work was funded by the Deutsche Forschungsgemeinschaft (DFG, German Research Foundation) in a TSPO research unit (ID 403161218) and under Germany's Excellence Strategy within the framework of the Munich Cluster for Systems Neurology (EXC 2145 SyNergy—ID 390857198) and CurePSP. The UCL team reports: National Institute for Health Research University College London Hospitals Biomedical Research Centre, AVID Radiopharmaceuticals (a wholly owned subsidiary of Eli Lilly). D.M.C. is supported by the UK Dementia Research Institute which receives its funding from DRI Ltd, funded by the UK Medical Research Council, Alzheimer's Society and Alzheimer's Research UK, Alzheimer's Association (SG-666374-UK BIRTH COHORT) and the National Institute for Health and Care Research University College London Hospitals Biomedical Research Centre. P.W. is funded by Wellcome Trust. The UCSF team reports: NIH/NIA (P30-AG062422, R01-AG045611 and R35-AG072362). The UPENN team reports: spreading tau in non-amnesic Alzheimer's disease (R01 AG054519), white matter contributions to tau spread cross AD clinical variants (Alzheimer's Association, AARG-22-926144), Penn Alzheimer's Disease Research Center (P30 AG072979). In addition, E.L. reports the following grants: P01AG066597, P01AG084497. The Washington team reports: Healthy Aging and Senile Dementia (P01 AG03991), Alzheimer's Disease Research Center (P30 AG066444), Adult Children Study (P01 AG026276), P30 NS04805, P30 NS098577, R01 AG043434, UL1 TR000448, R01 EB009352. The Yale team reports: P30AG047270, P30AG066508, P30AG021342, R01AG052560, R01AG062276. Additionally, C.F. reports: K23AG059919, the Alzheimer's Association (2019-AACSF-644153).

## Competing interests

C.G. (Amsterdam) is supported by a Dementia Fellowship grant from ZonMW (10510022110010). Y.A.L.P. (Amsterdam) has received funding from the Dutch Brain Foundation, ZonMW, NWO and the Mooiste Contact Fonds (both paid to her institution). N.F. (Munich) has received funding from the Alzheimer's Association, Bright Focus Foundation, Alzheimer Forschung Initiative, Schick Foundation, Avid Radiopharmaceuticals, Legerlotz Foundation and has received speaker honoraria from Eisai, Life Molecular Imaging, GE Healthcare and consulting honoraria from MSD. Projects of R.O. (Amsterdam) received support of the European Research Council, ZonMw, NWO, National Institute of Health, Alzheimer Association, Alzheimer

Nederland, Stichting Dioraphte, Cure Alzheimer's fund, Health Holland, ERA PerMed, Alzheimerfondsen, Hjärtfonden, Avid Radiopharmaceuticals, Janssen Research & Development, Roche, Quantarix and Optina Diagnostics. R.O. was a speaker at symposia organized by GE healthcare. R.O. is an advisory board member for Asceneuron, Bristol Myers Squibb and Biogen. All the aforementioned has been paid to the institutions. R.O. is part of the editorial board of Alzheimer's Research & Therapy and the European Journal of Nuclear Medicine and Molecular Imaging. M.M. (Cambridge) provides consultancy for Astex Pharmaceuticals (unrelated to this work). J.B.R. (Cambridge) reports: consultancy for Asceneuron, Alector, Astronautx, Astex, CumulusNeuro, Clinicalink, Curasen, Eisai, Ferrer, Prevail and SVHealth, unrelated to the current work. A.D. (Cologne) reports: research support by Siemens Healthineers, Life Molecular Imaging, GE Healthcare, AVID Radiopharmaceuticals, Sofie, Eisai, Novartis/AAA, Ariceum Therapeutics; Speaker Honorary/Advisory Boards: Siemens Healthineers, Sanofi, GE Healthcare, Biogen, Novo Nordisk, Invicro, Novartis/AAA, Bayer Vital, Lilly; Stock: Siemens Healthineers, Lantheus Holding, Structured therapeutics, Lilly; patents: patent for 18F-JK-PSMA-7 (Patent No.: EP3765097A1; Date of patent: 20 January, 2021). T.v.E. (Cologne) reports: advisory boards (ICON, Bial, Lundbeck Foundation), honoraria (Eisai, International Society for Parkinson and Movement Disorders, Korean Movement Disorders Society), consultancies (GT Gain Therapeutics SA, INSERM), grants (German Research Foundation, Humboldt Foundation, Brandau-Laibach Foundation). H.B. (Leipzig) received reader honoraria from Life Molecular Imaging, speaker honoraria from Novartis/AAA and IBA, dosing committee honoraria from Pharmtrace, and consulting honoraria from Lilly. O.H. (Lund) is an employee of Lund University and Eli Lilly. R.S. (Lund) has received speaker honoraria from Roche and Triolab. B.D.C.B. (Mayo) has received funding from Alzheimer Nederland (#WE.15-2019-13, #WE.03-2021-15, #WE.06-2023-01). P.R.N. (McGill) participated in Advisory Board for Roche, Novo Nordics and Cerveau (outside submitted work). J.T. (McGill) has served as a paid consultant for Neurotorium and for Alzheon Inc. M.B. (Munich) received speaker honoraria from Roche, Iba, GE Healthcare and Life Molecular Imaging, is an active advisor of MIAC, and advised GE Healthcare Life Molecular Imaging. J.L. (Munich) reports speaker fees from Bayer Vital, Biogen, EISAI, TEVA, Zambon, Esteve, Merck and Roche, consulting fees from Axon Neuroscience, EISAI and Biogen, author fees from Thieme medical publishers and W. Kohlhammer GmbH medical publishers and is inventor in a patent 'Oral Phenylbutyrate for Treatment of Human 4-Repeat Tauopathies' (PCT/EP2024/053388) filed by LMU Munich. In addition, he reports compensation for serving as chief medical officer for MODAG GmbH, is beneficiary of the phantom share program of MODAG GmbH and is inventor of a patent 'Pharmaceutical Composition and Methods of Use' (EP 22 159 408.8) filed by MODAG GmbH, all activities outside the submitted work. D.M.C. (UCL) reports a paid consultancy with Perceptive Imaging. J.M.S. (UCL) has received research funding and PET tracer from AVID Radiopharmaceuticals (a wholly owned subsidiary of Eli Lilly) and Alliance Medical; has consulted for Roche, Eli Lilly, Biogen, AVID, Merck and GE; and received royalties from Oxford University Press and Henry Stewart Talks. He is Chief Medical Officer for Alzheimer's Research UK. R.L.J. (UCSF) consulted for GE Healthcare. G.D.R. (UCSF) receives research support from Avid Radiopharmaceuticals, GE Healthcare, Life Molecular Imaging, Genentech. He has served as a paid consultant for Alector, Eli Lilly, Johnson & Johnson, Merck. He is a member of the AD Therapeutics Workgroup and an Associate Editor for JAMA Neurology. E.B.L. (UPENN) has received consulting fees from Lilly and Wavebreak

Therapeutics. R.S.O. (Yale) reports grants for clinical trials from Cognition Therapeutics and Bristol-Myers Squibb outside of the submitted work. The other authors report no competing interests.

## Supplementary material

Supplementary material is available at [Brain](https://brain.oup.com/brain/article/148/11/3893/8234281) online.

## References

- Braak H, Braak E. Neuropathological staging of Alzheimer-related changes. *Acta Neuropathol.* 1991;82:239–259.
- Ossenkoppele R, Pichet Binette A, Groot C, et al. Amyloid and tau PET-positive cognitively unimpaired individuals are at high risk for future cognitive decline. *Nat Med.* 2022;28:2381–2387.
- Jack CR, Knopman DS, Jagust WJ, et al. Tracking pathophysiological processes in Alzheimer's disease: An updated hypothetical model of dynamic biomarkers. *Lancet Neurol.* 2013;12:207–216.
- La Joie R, Visani AV, Baker SL, et al. Prospective longitudinal atrophy in Alzheimer's disease correlates with the intensity and topography of baseline tau-PET. *Sci Transl Med.* 2020;12:eaa5732.
- Ossenkoppele R, Iaccarino L, Schonhaut DR, et al. Tau covariance patterns in Alzheimer's disease patients match intrinsic connectivity networks in the healthy brain. *Neuroimage Clin.* 2019;23:101848.
- Franzmeier N, Rubinski A, Neitzel J, et al. Functional connectivity associated with tau levels in ageing, Alzheimer's, and small vessel disease. *Brain.* 2019;142:1093–1107.
- Franzmeier N, Dewenter A, Frontzkowski L, et al. Patient-centered connectivity-based prediction of tau pathology spread in Alzheimer's disease. *Sci Adv.* 2020;6:eabd1327.
- Franzmeier N, Neitzel J, Rubinski A, et al. Functional brain architecture is associated with the rate of tau accumulation in Alzheimer's disease. *Nat Commun.* 2020;11:347.
- Wu JW, Hussaini SA, Bastille IM, et al. Neuronal activity enhances tau propagation and tau pathology in vivo. *Nat Neurosci.* 2016;19:1085–1092.
- Mudher A, Colin M, Dujardin S, et al. What is the evidence that tau pathology spreads through prion-like propagation? *Acta Neuropathol Commun.* 2017;5:99.
- He ZH, McBride JD, Xu H, et al. Transmission of tauopathy strains is independent of their isoform composition. *Nat Commun.* 2020;11:7.
- Jucker M, Walker LC. Propagation and spread of pathogenic protein assemblies in neurodegenerative diseases. *Nat Neurosci.* 2018;21:1341–1349.
- Sintini I, Graff-Radford J, Jones DT, et al. Tau and amyloid relationships with resting-state functional connectivity in atypical Alzheimer's disease. *Cereb Cortex.* 2021;31:1693–1706.
- Katsumi Y, Putcha D, Eckbo R, et al. Anterior dorsal attention network tau drives visual attention deficits in posterior cortical atrophy. *Brain.* 2023;146:295–306.
- Schoonhoven DN, Coomans EM, Millán AP, et al. Tau protein spreads through functionally connected neurons in Alzheimer's disease: A combined MEG/PET study. *Brain.* 2023;146:4040–4054.
- Therriault J, Pascoal TA, Savard M, et al. Intrinsic connectivity of the human brain provides scaffold for tau aggregation in clinical variants of Alzheimer's disease. *Sci Transl Med.* 2022;14:eabc8693.
- Adams JN, Maass A, Harrison TM, Baker SL, Jagust WJ. Cortical tau deposition follows patterns of entorhinal functional connectivity in aging. *Elife.* 2019;8:e49132.
- de Flores R, Das SR, Xie L, et al. Medial temporal lobe networks in Alzheimer's disease: Structural and molecular vulnerabilities. *J Neurosci.* 2022;42:2131–2141.
- Vogel JW, Iturria-Medina Y, Strandberg OT, et al. Spread of pathological tau proteins through communicating neurons in human Alzheimer's disease. *Nat Commun.* 2020;11:2612.
- Vogel JW, Young AL, Oxtoby NP, et al. Four distinct trajectories of tau deposition identified in Alzheimer's disease. *Nat Med.* 2021;27:871–881.
- Lee WJ, Brown JA, Kim HR, et al. Regional A $\beta$ -tau interactions promote onset and acceleration of Alzheimer's disease tau spreading. *Neuron.* 2022;110:1932–1943.
- Wang Y, Balaji V, Kaniyappan S, et al. The release and trans-synaptic transmission of tau via exosomes. *Mol Neurodegener.* 2017;12:5.
- Tardivel M, Bégar S, Bousset L, et al. Tunneling nanotube (TNT)-mediated neuron-to-neuron transfer of pathological tau protein assemblies. *Acta Neuropathol Commun.* 2016;4:117.
- Ahmed Z, Cooper J, Murray TK, et al. A novel in vivo model of tau propagation with rapid and progressive neurofibrillary tangle pathology: The pattern of spread is determined by connectivity, not proximity. *Acta Neuropathol.* 2014;127:667–683.
- Dujardin S, Lécolle K, Caillierez R, et al. Neuron-to-neuron wild-type tau protein transfer through a trans-synaptic mechanism: Relevance to sporadic tauopathies. *Acta Neuropathol Commun.* 2014;2:14.
- Iba M, McBride JD, Guo JL, Zhang B, Trojanowski JQ, Lee VM-Y. Tau pathology spread in PS19 tau transgenic mice following locus coeruleus (LC) injections of synthetic tau fibrils is determined by the LC's afferent and efferent connections. *Acta Neuropathol.* 2015;130:349–362.
- Zhou J, Gennatas ED, Kramer JH, Miller BL, Seeley WW. Predicting regional neurodegeneration from the healthy brain functional connectome. *Neuron.* 2012;73:1216–1227.
- Mrdjen D, Fox EJ, Bukhari SA, Montine KS, Bendall SC, Montine TJ. The basis of cellular and regional vulnerability in Alzheimer's disease. *Acta Neuropathol.* 2019;138:729–749.
- Sanchez JS, Becker JA, Jacobs HL, et al. The cortical origin and initial spread of medial temporal tauopathy in Alzheimer's disease assessed with positron emission tomography. *Sci Transl Med.* 2021;13:eabc0655.
- Schöll M, Lockhart SN, Schonhaut DR, et al. PET imaging of tau deposition in the aging human brain. *Neuron.* 2016;89:971–982.
- Johnson KA, Schultz A, Betensky RA, et al. Tau positron emission tomographic imaging in aging and early Alzheimer disease. *Ann Neurol.* 2016;79:110–119.
- St-Onge F, Chapleau M, Breitner JCS, Villeneuve S, Pichet Binette A. Tau accumulation and its spatial progression across the Alzheimer's disease spectrum. *Brain Commun.* 2024;6:fcae031.
- Therriault J, Pascoal TA, Lussier FZ, et al. Biomarker modeling of Alzheimer's disease using PET-based Braak staging. *Nat Aging.* 2022;2:526–535.
- Biel D, Brendel M, Rubinski A, et al. Tau-PET and in vivo Braak-staging as prognostic markers of future cognitive decline in cognitively normal to demented individuals. *Alzheimers Res Ther.* 2021;13:137.
- Crutch SJ, Lehmann M, Schott JM, Rabinovici GD, Rossor MN, Fox NC. Posterior cortical atrophy. *Lancet Neurol.* 2012;11:170–178.
- Gorno-Tempini ML, Hillis AE, Weintraub S, et al. Classification of primary progressive aphasia and its variants. *Neurology.* 2011;76:1006–1014.
- Ossenkoppele R, Pijnenburg YAL, Perry DC, et al. The behavioural/dysexecutive variant of Alzheimer's disease: Clinical,



- neuroimaging and pathological features. *Brain*. 2015;138:2732–2749.
38. Armstrong MJ, Litvan I, Lang AE, et al. Criteria for the diagnosis of corticobasal degeneration. *Neurology*. 2013;80:496–503.
  39. Murray ME, Graff-Radford NR, Ross OA, Petersen RC, Duara R, Dickson DW. Neuropathologically defined subtypes of Alzheimer's disease with distinct clinical characteristics: A retrospective study. *Lancet Neurol*. 2011;10:785–796.
  40. Ossenkoppele R, Schonhaut DR, Schöll M, et al. Tau PET patterns mirror clinical and neuroanatomical variability in Alzheimer's disease. *Brain*. 2016;139:1551–1567.
  41. Tosun D, Thropp P, Southekal S, Spottiswoode B, Fahmi R. Profiling and predicting distinct tau progression patterns: An unsupervised data-driven approach to flortaucipir positron emission tomography. *Alzheimers Dement*. 2023;19:5605–5619.
  42. Palleis C, Brendel M, Finze A, et al. Cortical [F]PI-2620 binding differentiates corticobasal syndrome subtypes. *Mov Disord*. 2021;36:2104–2115.
  43. Cho H, Mundada NS, Apostolova LG, et al. Amyloid and tau-PET in early-onset AD: Baseline data from the longitudinal early-onset Alzheimer's disease study (LEADS). *Alzheimers Dement*. 2023;19(Suppl 9): S98–S114.
  44. Boon BDC, Frigerio I, de Gooijer D, et al. Alzheimer's disease clinical variants show distinct neuroinflammatory profiles with neuropathology. *Neuropathol Appl Neurobiol*. 2024;50: e13009.
  45. Graff-Radford J, Yong KXX, Apostolova LG, et al. New insights into atypical Alzheimer's disease in the era of biomarkers. *Lancet Neurol*. 2021;20:222–234.
  46. Polsinelli AJ, Apostolova LG. Atypical Alzheimer disease variants. *Continuum (Minneapolis)*. 2022;28:676–701.
  47. Singleton E, Hansson O, Pijnenburg YAL, et al. Heterogeneous distribution of tau pathology in the behavioural variant of Alzheimer's disease. *J Neurol Neurosurg Psychiatry*. 2021;92:872–880.
  48. Holland N, Savulich G, Jones PS, et al. Differential synaptic loss in beta-amyloid positive versus beta-amyloid negative corticobasal syndrome. *Mov Disord*. 2024;39:1166–1178.
  49. Dilcher R, Wall S, Groß M, et al. Combining cerebrospinal fluid and PI-2620 tau-PET for biomarker-based stratification of Alzheimer's disease and 4R-tauopathies. *Alzheimers Dement*. 2024;20:6896–6909.
  50. Dronse J, Fliessbach K, Bischof GN, et al. In vivo patterns of tau pathology, amyloid-beta burden, and neuronal dysfunction in clinical variants of Alzheimer's disease. *J Alzheimers Dis*. 2017;55:465–471.
  51. Sintini I, Graff-Radford J, Schwarz CG, et al. Longitudinal rates of atrophy and tau accumulation differ between the visual and language variants of atypical Alzheimer's disease. *Alzheimers Dement*. 2023;19:4396–4406.
  52. Weston PSJ, Coath W, Harris MJ, et al. Cortical tau is associated with microstructural imaging biomarkers of neurite density and dendritic complexity in Alzheimer's disease. *Alzheimers Dement*. 2023;19:2750–2754.
  53. Brendel M, Barthel H, van Eimeren T, et al. Assessment of 18F-PI-2620 as a biomarker in progressive supranuclear palsy. *JAMA Neurol*. 2020;77:1408–1419.
  54. Day GS, Gordon BA, Jackson K, et al. Tau-PET binding distinguishes patients with early-stage posterior cortical atrophy from amnesic Alzheimer disease dementia. *Alzheimer Dis Assoc Disord*. 2017;31:87–93.
  55. Ossenkoppele R, Reimand J, Smith R, et al. Tau PET correlates with different Alzheimer's disease-related features compared to CSF and plasma p-tau biomarkers. *EMBO Mol Med*. 2021;13: e14398.
  56. Phillips JS, Das SR, McMillan CT, et al. Tau PET imaging predicts cognition in atypical variants of Alzheimer's disease. *Hum Brain Mapp*. 2018;39:691–708.
  57. Abuwarda H, Trainer A, Horien C, et al. Whole-brain functional connectivity predicts regional tau PET in preclinical Alzheimer's disease. *bioRxiv*. [Preprint] doi:10.1101/2024.04.02.587791
  58. Schaefer A, Kong R, Gordon EM, et al. Local-global parcellation of the human cerebral cortex from intrinsic functional connectivity MRI. *Cereb Cortex*. 2018;28:3095–3114.
  59. Franzmeier N, Dehsarvi A, Steward A, et al. Elevated CSF GAP-43 is associated with accelerated tau accumulation and spread in Alzheimer's disease. *Nat Commun*. 2024;15:202.
  60. Kim B, Suh E, Nguyen AT, et al. TREM2 risk variants are associated with atypical Alzheimer's disease. *Acta Neuropathol*. 2022;144:1085–1102.
  61. Petersen C, Nolan AL, de Paula França Resende E, et al. Alzheimer's disease clinical variants show distinct regional patterns of neurofibrillary tangle accumulation. *Acta Neuropathol*. 2019;138:597–612.
  62. Kovacs GG, Lukic MJ, Irwin DJ, et al. Distribution patterns of tau pathology in progressive supranuclear palsy. *Acta Neuropathol*. 2020;140:99–119.
  63. Amunts K, Mohlberg H, Bludau S, Zilles K. Julich-brain: A 3D probabilistic atlas of the human brain's cytoarchitecture. *Science*. 2020;369:988–992.
  64. The Computational Brain Anatomy (CoBRA) Laboratory. Accessed 30 May 2025. <https://www.cobralab.ca/>
  65. Neuromorphometrics, Inc. Building a Model of the Living Human Brain. Accessed 30 May 2025. <https://www.neuromorphometrics.com/>
  66. Rolls ET, Huang CC, Lin CP, Feng JF, Joliot M. Automated anatomical labelling atlas 3. *Neuroimage*. 2020;206:116189.
  67. Franzmeier N, Brendel M, Beyer L, et al. Tau deposition patterns are associated with functional connectivity in primary tauopathies. *Nat Commun*. 2022;13:1362.
  68. Yeo BTT, Krienen FM, Sepulcre J, et al. The organization of the human cerebral cortex estimated by intrinsic functional connectivity. *J Neurophysiol*. 2011;106:1125–1165.
  69. Leuzy A, Raket LL, Villemagne VL, et al. Harmonizing tau positron emission tomography in Alzheimer's disease: The CenTauR scale and the joint propagation model. *Alzheimers Dement*. 2024;20:5833–5848.
  70. Tang-Wai DF, Graff-Radford NR, Boeve BF, et al. Clinical, genetic, and neuropathologic characteristics of posterior cortical atrophy. *Neurology*. 2004;63:1168–1174.
  71. Chapleau M, La Joie R, Yong K, et al. Demographic, clinical, biomarker, and neuropathological correlates of posterior cortical atrophy: An international cohort study and individual participant data meta-analysis. *Lancet Neurol*. 2024;23:168–177.
  72. Josephs KA, Martin PR, Botha H, et al. [<sup>18</sup>F]AV-1451 tau-PET and primary progressive aphasia. *Ann Neurol*. 2018;83:599–611.
  73. Mesulam MM, Rogalski EJ, Wieneke C, et al. Primary progressive aphasia and the evolving neurology of the language network. *Nat Rev Neurol*. 2014;10:554–569.
  74. Lee SE, Rabinovici GD, Mayo MC, et al. Clinicopathological correlations in corticobasal degeneration. *Ann Neurol*. 2011;70: 327–340.
  75. Sakae N, Josephs KA, Litvan I, et al. Clinicopathologic subtype of Alzheimer's disease presenting as corticobasal syndrome. *Alzheimers Dement*. 2019;15:1218–1228.
  76. Aguero C, Dhaynaut M, Amaral AC, et al. Head-to-head comparison of [<sup>18</sup>F]-Flortaucipir, [<sup>18</sup>F]-MK-6240 and [<sup>18</sup>F]-PI-2620 postmortem binding across the spectrum of neurodegenerative diseases. *Acta Neuropathol*. 2024;147:25.

77. Baker SL, Harrison TM, Maass A, La Joie R, Jagust WJ. Effect of off-target binding on F-flortaucipir variability in healthy controls across the life span. *J Nucl Med*. 2019;60:1444–1451.
78. Scheinost D, Chang J, Lacadie C, et al. Functional connectivity for the language network in the developing brain: 30 weeks of gestation to 30 months of age. *Cereb Cortex*. 2022;32:3289–3301.
79. Frontzkowski L, Ewers M, Brendel M, et al. Earlier Alzheimer's disease onset is associated with tau pathology in brain hub regions and facilitated tau spreading. *Nat Commun*. 2022;13:4899.
80. Condello C, Westaway D, Prusiner SB. Expanding the prion paradigm to include Alzheimer and Parkinson diseases. *JAMA Neurol*. 2024;81:1023–1024.
81. Brettschneider J, Del Tredici K, Lee VM, Trojanowski JQ. Spreading of pathology in neurodegenerative diseases: A focus on human studies. *Nat Rev Neurosci*. 2015;16:109–120.
82. Honey CJ, Sporns O, Cammoun L, et al. Predicting human resting-state functional connectivity from structural connectivity. *Proc Natl Acad Sci USA*. 2009;106:2035–2040.
83. Polanco JC, Scicluna BJ, Hill AF, Götz J. Extracellular vesicles isolated from the brains of rTg4510 mice seed tau protein aggregation in a threshold-dependent manner. *J Biol Chem*. 2016;291:12445–12466.
84. Abounit S, Wu JW, Duff K, Victoria GS, Zurzolo C. Tunneling nanotubes: A possible highway in the spreading of tau and other prion-like proteins in neurodegenerative diseases. *Prion*. 2016;10:344–351.
85. Holmes BB, DeVos SL, Kfoury N, et al. Heparan sulfate proteoglycans mediate internalization and propagation of specific proteopathic seeds. *Proc Natl Acad Sci USA*. 2013;110:E3138–E3147.
86. Takahashi M, Miyata H, Kametani F, et al. Extracellular association of APP and tau fibrils induces intracellular aggregate formation of tau. *Acta Neuropathol*. 2015;129:895–907.
87. Gómez-Ramos A, Díaz-Hernández M, Rubio A, Miras-Portugal MT, Avila J. Extracellular tau promotes intracellular calcium increase through M1 and M3 muscarinic receptors in neuronal cells. *Mol Cell Neurosci*. 2008;37:673–681.
88. Gómez-Ramos A, Díaz-Hernández M, Rubio A, Díaz-Hernández JI, Miras-Portugal MT, Avila J. Characteristics and consequences of muscarinic receptor activation by tau protein. *Eur Neuropsychopharm*. 2009;19:708–717.
89. Clavaguera F, Bolmont T, Crowther RA, et al. Transmission and spreading of tauopathy in transgenic mouse brain. *Nat Cell Biol*. 2009;11:909–913.
90. Peeraer E, Bottelbergs A, Van Kolen K, et al. Intracerebral injection of preformed synthetic tau fibrils initiates widespread tauopathy and neuronal loss in the brains of tau transgenic mice. *Neurobiol Dis*. 2015;73:83–95.
91. de Calignon A, Polydoro M, Suárez-Calvet M, et al. Propagation of tau pathology in a model of early Alzheimer's disease. *Neuron*. 2012;73:685–697.
92. Liu L, Drouet V, Wu JW, et al. Trans-synaptic spread of tau pathology in vivo. *PLoS One*. 2012;7:e31302.
93. Holmes BB, Furman JL, Mahan TE, et al. Proteopathic tau seeding predicts tauopathy in vivo. *Proc Natl Acad Sci USA*. 2014;111:E4376–E4385.
94. Asai H, Ikezu S, Tsunoda S, et al. Depletion of microglia and inhibition of exosome synthesis halt tau propagation. *Nat Neurosci*. 2015;18:1584–1593.
95. Wegmann S, Maury EA, Kirk MJ, et al. Removing endogenous tau does not prevent tau propagation yet reduces its neurotoxicity. *EMBO J*. 2015;34:3028–3041.
96. Clavaguera F, Hench J, Lavenir I, et al. Peripheral administration of tau aggregates triggers intracerebral tauopathy in transgenic mice. *Acta Neuropathol*. 2014;127:299–301.
97. Clavaguera F, Akatsu H, Fraser G, et al. Brain homogenates from human tauopathies induce tau inclusions in mouse brain. *Proc Natl Acad Sci USA*. 2013;110:9535–9540.
98. Giorgio J, Adams JN, Maass A, Jagust WJ, Breakspear M. Amyloid induced hyperexcitability in default mode network drives medial temporal hyperactivity and early tau accumulation. *Neuron*. 2024;112:676–686.e4.
99. Leuzy A, Binette AP, Vogel JW, et al. Comparison of group-level and individualized brain regions for measuring change in longitudinal tau positron emission tomography in Alzheimer disease. *JAMA Neurol*. 2023;80:614–623.
100. Vermeiren MR, Calandri IL, van der Flier WM, van de Giessen E, Ossenkoppele R. Survey among experts on the future role of tau-PET in clinical practice and trials. *Alzheimers Dement-Datm*. 2024;16:e70033.
101. Theriault J, Schindler SE, Salvadó G, et al. Biomarker-based staging of Alzheimer disease: Rationale and clinical applications. *Nat Rev Neurol*. 2024;20:232–244.
102. Janelidze S, Pannee J, Mikulskis A, et al. Concordance between different amyloid immunoassays and visual amyloid positron emission tomographic assessment. *JAMA Neurol*. 2017;74:1492–1501.
103. Phillips JS, Nitchie FJ, Da Re F, et al. Rates of longitudinal change in (18)F-flortaucipir PET vary by brain region, cognitive impairment, and age in atypical Alzheimer's disease. *Alzheimers Dement*. 2022;18:1235–1247.
104. Kaufman SK, Del Tredici K, Thomas TL, Braak H, Diamond MI. Tau seeding activity begins in the transentorhinal/entorhinal regions and anticipates phospho-tau pathology in Alzheimer's disease and PART. *Acta Neuropathol*. 2018;136:57–67.
105. Rogalski E, Johnson N, Weintraub S, Mesulam M. Increased frequency of learning disability in patients with primary progressive aphasia and their first-degree relatives. *Arch Neurol*. 2008;65:244–248.
106. Miller ZA, Mandelli ML, Rankin KP, et al. Handedness and language learning disability differentially distribute in progressive aphasia variants. *Brain*. 2013;136:3461–3473.
107. Miller ZA, Rosenberg L, Santos-Santos MA, et al. Prevalence of mathematical and visuospatial learning disabilities in patients with posterior cortical atrophy. *JAMA Neurol*. 2018;75:728–737.
108. Mesulam MM. Primary progressive aphasia and the language network: The 2013 H. Houston Merritt lecture. *Neurology*. 2013;81:456–462.
109. Sun AY, Nguyen XV, Bing GY. Comparative analysis of an improved thioflavin-S stain, gallyas silver stain, and immunohistochemistry for neurofibrillary tangle demonstration on the same sections. *J Histochem Cytochem*. 2002;50:463–472.
110. Otvos L, Feiner L, Lang E, Szendrei GI, Goedert M, Lee VM-Y. Monoclonal-antibody Phf-1 recognizes tau-protein phosphorylated at serine residue-396 and residue-404. *J Neurosci Res*. 1994;39:669–673.
111. Leuzy A, Chiotis K, Lemoine L, et al. Tau PET imaging in neurodegenerative tauopathies—still a challenge. *Mol Psychiatry*. 2019;24:1112–1134.
112. Moses WW. Fundamental limits of spatial resolution in PET. *Nucl Instrum Methods Phys Res A*. 2011;648:S236–S240.
113. Walsh DM, Selkoe DJ. A critical appraisal of the pathogenic protein spread hypothesis of neurodegeneration. *Nat Rev Neurosci*. 2016;17:251–260.
114. Richiardi J, Altmann A, Milazzo A-C, et al. Correlated gene expression supports synchronous activity in brain networks. *Science*. 2015;348:1241–1244.

115. Chand P, Grafman J, Dickson D, Ishizawa K, Litvan I. Alzheimer's disease presenting as corticobasal syndrome. *Mov Disord*. 2006;21:2018-2022.
116. Koga S, Josephs KA, Aiba I, Yoshida M, Dickson DW. Neuropathology and emerging biomarkers in corticobasal syndrome. *J Neurol Neurosurg Psychiatry*. 2022;93:919-929.
117. Lehmann M, Ghosh PM, Madison C, et al. Diverging patterns of amyloid deposition and hypometabolism in clinical variants of probable Alzheimer's disease. *Brain*. 2013;136: 844-858.
118. Martersteck A, Ayala I, Ohm DT, et al. Focal amyloid and asymmetric tau in an imaging-to-autopsy case of clinical primary progressive aphasia with Alzheimer disease neuropathology. *Acta Neuropathol Commun*. 2022;10:111.
119. Ramirez J, Saleh IG, Yanagawa ESK, et al. Multivalency drives interactions of alpha-synuclein fibrils with tau. *PLoS One*. 2024;19:e0309416.
120. Tomé SO, Tsaka G, Ronisz A, et al. TDP-43 pathology is associated with increased tau burdens and seeding. *Mol Neurodegener*. 2023; 18:71.